A Study of Electrochemical Impedance Spectroscopy of β-alumina $Na_2O \cdot 11Al_2O_3$ and NASICON Type $Li_{1.3}Al_{0.3}Ti_{1.7}(PO_4)_3$

by

Zhicheng Zhao

A thesis submitted to the Graduate Faculty of
Auburn University
in partial fulfillment of the
requirements for the Degree of
Master of Science

Auburn, Alabama
May 4, 2019

Keywords: EIS, solid electrolyte, equivalent circuit,

Approved by

Jeffrey Fergus, Chair, Professor of Materials Engineering
Dong-Joo Kim, Professor of Materials Engineering
Majid Beidaghi, Assistant Professor of Materials Engineering

Abstract

Solid electrolytes are functional materials with high ionic conductivity. The conductivity highly depends on the microstructure such as grains and grain boundaries. For most solid electrolytes, both grain and grain boundary contribute to the conductivity. In order to better understand the conductive mechanism, it is important to identify the contribution of grain and grain boundary. Electrochemical impedance spectroscopy (EIS) was used to measure the impedance of β-alumina $Na_2O{\cdot}11Al_2O_3$ and NASICON type $Li_{1.3}Al_{0.3}Ti_{1.7}(PO_4)_3$ (LATP) by the impedance complex plan. Activation energy is an important factor to identify materials. The bulk property and grain boundary property were distinguished according to the activation energy of each property. An equivalent circuit which contains external influence factor components was built to simulate the electrical properties to make the electrical properties of each electrolyte much accurate. The fitting results show high coincidence with the origin plots obtained by the EIS test. The physical significance of the equivalent circuit is explained theoretically and experimentally.

Acknowledgments

I would like to thank everyone who gave me encouragement and help during my entire study and daily life at Auburn University.

Table of Contents

List of Tables

List of Figures

Chapter 1

Introduction

1.1 Solid Electrolyte

A solid electrolyte or superionic conductor is a conductive material composed of one or more than one ionic compound, and it has high ionic conductivity at room temperature. Unlike liquid ionic conductors, only one of the two oppositely charged ions is movable in a solid electrolyte, the other ion constitutes the structure of the crystal or ion migration tunnels. The movement of the movable ions in the solid electrolyte is usually due to the existence of point defects or ion migration tunnels and the large amplitude of its vibration in the crystal lattice. Solid electrolytes are useful materials that can be used in batteries and sensors because of the high ionic conductivity.

1.2 Electrochemical Impedance Spectroscopy

When the potential or current applied on an electrode system changes, the corresponding current or potential output from the electrode system also changes accordingly. This situation is the same as a current or voltage response when a circuit is subjected to a voltage or current disturbance signal. When a stable electrode system is disturbed with a sinusoidal current signal of a sufficient small amplitude with an angular frequency of ω, the corresponding electrode potential produces a sinusoidal response with an angular frequency of ω. The response is measured, and the impedance is output at each frequency. [1]

$$Z_\omega = E_\omega / I_\omega \qquad (1.2.1)$$

Where E_ω is frequency-dependent potential, I_ω is frequency-dependent current, and Z_ω is frequency-dependent impedance. The set of such frequency response function values measured at a series of different angular frequencies is the electrochemical impedance spectrum of the electrode system.

The study on solid electrolytes by electrochemical impedance spectroscopy can help understand the conductive mechanism of conductive ions and the contribution of different carriers to conductivity. The effects of structure and preparation process on properties and the electrochemical processes involving solid electrolytes can also be shown. EIS also has a disadvantage. Sometimes, one impedance spectrum can be fitted by different equivalent circuits. Thus, the equivalent circuit applied may not be reliable if the physical significance of components is not realistic.

1.3 Equivalent Circuit Components

After obtaining the electrochemical impedance spectrum of an electrode system, some electrical components could be used to form a circuit to make the impedance spectrum of the circuit be the same as the measured electrochemical impedance spectrum of the electrode system. This circuit is referred to as an equivalent circuit of the electrode system or electrode process. The components used to constitute the equivalent circuit are referred to as equivalent components.

There are basically four kinds of equivalent components, equivalent resistance (R), equivalent inductance (L), equivalent capacitance (C) and constant phase element (CPE).

The impedance of the resistor (R) only has the real part, but it does not have the imaginary part. The value of the impedance is positive, and it is independent of the frequency. In the impedance complex plan, the resistance can only be represented by a point on the real axis.

$$Z'_R=R \qquad Z''_R=0 \qquad (1.3.1)$$

The impedance of the inductor (L) only has the imaginary part, but it does not have the real part. The value of the impedance is positive. In the impedance complex plan, it is represented as a line that coincides with the longitudinal axis of the fourth quadrant.

$$Z'_L=0 \qquad Z''_L=\omega L \qquad (1.3.2)$$

The impedance of the capacitor (C) only has the imaginary part, but it does not have the real part. The value of the impedance is positive. In the impedance complex plane, it is represented as a line that coincides with the longitudinal axis of the first quadrant.

$$Z'_C=0 \qquad Z''_C=-1/(\omega C) \qquad (1.3.3)$$

An electric double layer at the interface between the electrode and the electrolyte, generally equivalent to a capacitor, is called a double layer capacitor. [2] However, it was found in the experiment that the frequency response characteristics of the double layer capacitor of the solid electrode are inconsistent with the pure capacitance. The capacitive characteristics often show different degrees of frequency dispersion. A possible reason for this phenomenon is because of the roughness of the double layer surface. This common phenomenon is called dispersion effect. In the practical experiment, an ideal capacitance (C) is usually replaced by a constant phase element (CPE) due to the roughness of the two parallel surfaces. The CPE has both the real part and the imaginary part. In the impedance complex plan, it is represented as a depressed semicircle when parallel with a resistance. [3]

Warburg impedance (W) is another important element. It usually exists in the irreversible electrochemical process with redox reactions. The reason for Warburg impedance is the diffusion of reactants from the electrolyte to the electrode. In the irreversible electrochemical process, there are redox reactions occur on the solution-electrode surface. The reactants are consumed on the surface as the reaction goes on. This causes a concentration difference of reactants between the solution-electrode interface and the electrolyte. The reactants in the electrolyte diffuse to the solution-electrolyte interface due to the concentration difference to keep the reaction going. This diffusion process could be reflected on the impedance complex plane at a low-frequency region which is presented as a slash with 45°. [4] In the experiments of this thesis, there is no redox reaction at electrodes, thus the Warburg element is not applied in the equivalent circuit.

1.4 General Equivalent Circuit

In order to obtain numerical data of electrical properties of the electrolyte such as the resistance and the capacitance, an electric circuit must be established to simulate the electrical properties of the electrolyte. The response spectrum of the equivalent circuit needs to be identical with that of the electrolyte. Also, each part of the equivalent circuit should have the right physical significance according to the practical process.

In the practical EIS test, there are always some external influence factors, such as wires and electrodes. These elements do not belong to the electrolyte, but their electrical properties may also be expressed on the impedance plot, such as the inductance and the capacitance. In other words, the electrical properties revealed by the impedance plot contains factors of electrolyte and those of no relation to the electrolyte. In order to eliminate the deviation caused by the external

factors, some circuit components which are not related to the electrolyte need to be applied in the equivalent circuit.

A general equivalent circuit was built and applied for the two types of solid electrolyte in this thesis. The equivalent circuit is shown in Figure 1. The establishment details of the equivalent circuit will be explained in chapter 4 combined with the micromodel of the electrolyte-electrode system.

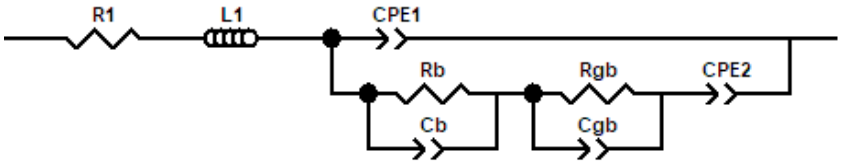

Figure 1. General equivalent circuit.

The equivalent circuit has two parts. The components which represent the electrolyte includes Rb, Cb, Rgb, and Cgb, where Rb is bulk resistance, Cb is bulk capacitance, Rgb is grain boundary resistance, Cgb is grain boundary capacitance. The components which represent the external factors include R1, L1, CPE1, and CPE2, where R1 is system resistance, L1 is inductance caused by wire bending, CPE1 is geometrical capacitance due to the electrolyte between the two parallel metal electrodes, CPE2 is interface capacitance caused by two electrolyte-electrode interfaces. This equivalent circuit can be simplified according to the practical process and impedance spectrum obtained. More details will be discussed in chapter 4.

Chapter 2

Literature review

For β-Alumina $Na_2O \cdot 11Al_2O_3$, Powers and Mitoff [5] reported a simplified model shown in Figure 2, which shows a good approximation of the electrical properties of β-alumina ceramic, where r_c is the resistance of grain, r_b is the resistance of grain boundaries, c_b is the capacitance of grain boundaries.

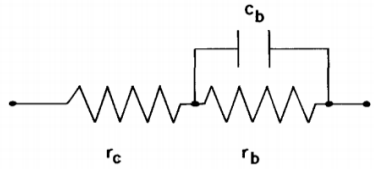

Figure 2. Powers's model for the electrical properties of polycrystalline β-alumina.

Hooper [6] reported an improved equivalent circuit model shown in Figure 3, which contains electrode-electrolyte interface capacitance (C_{dl}). The circuit well represents a double layer phenomenon at the interface.

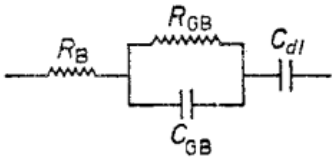

Figure 3. Hooper's model for the electrical properties of polycrystalline β-alumina.

Jonghe [7] described the electrode system using a similar model shown in Figure 4, which contains two interfacial capacitors (C_e) that represent two electrode-electrolyte interfaces at both sides of the electrolyte.

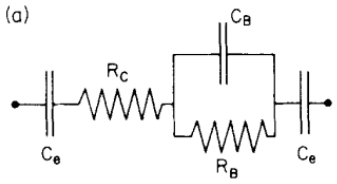

Figure 4. Jonghe's model for the electrical properties of polycrystalline β-alumina.

For NASICON Type $Li_{1.3}Al_{0.3}Ti_{1.7}(PO_4)_3$ (LATP), Duluard [8] performed the conductivity test of a powder sample without sintering. The impedance plot was fitted by using a simple model similar to Powers and Mitoff's model shown in Figure 5, where R_1 is the resistance of the measurement system, R_2 is the resistance of the electrolyte, constant phase element (CPE) that corresponds to grain boundary takes the place of the capacitor.

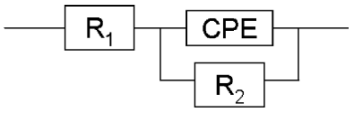

Figure 5. Duluard's equivalent circuit.

Zhao [9] fitted the impedance plot using a model similar to Hooper's model shown in Figure 6. Constant phase element (CPE_1) that correspond to the grain boundary takes the place of the C_{GB}, constant phase element (CPE_2) that correspond to the double layer takes the place of C_{dl}.

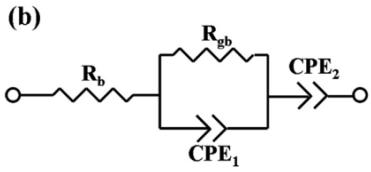

Figure 6. Zhao's equivalent circuit.

Arrhenius plots of β-Alumina and LATP conductivity of researchers' results are shown in Figure 7-8.

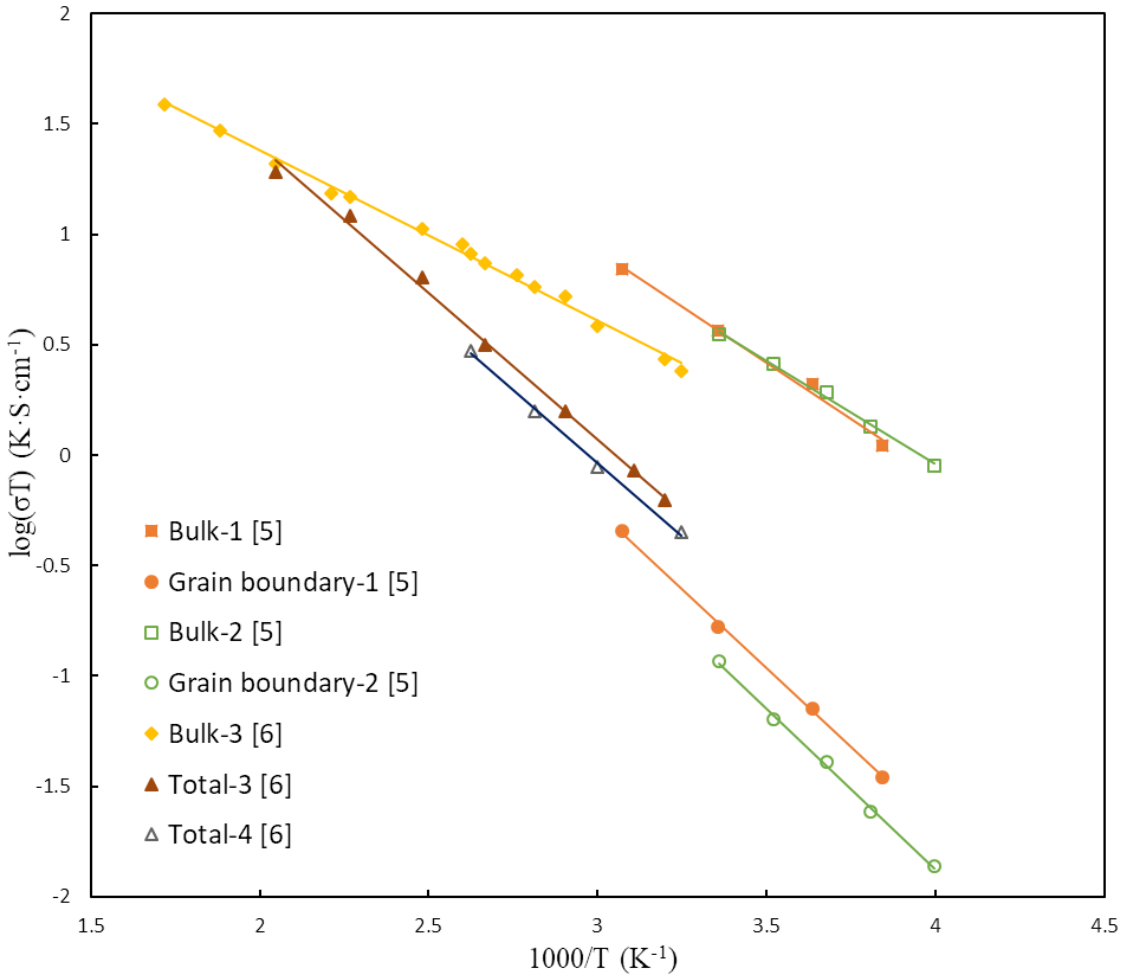

Figure 7. Arrhenius plots of β-alumina conductivity.

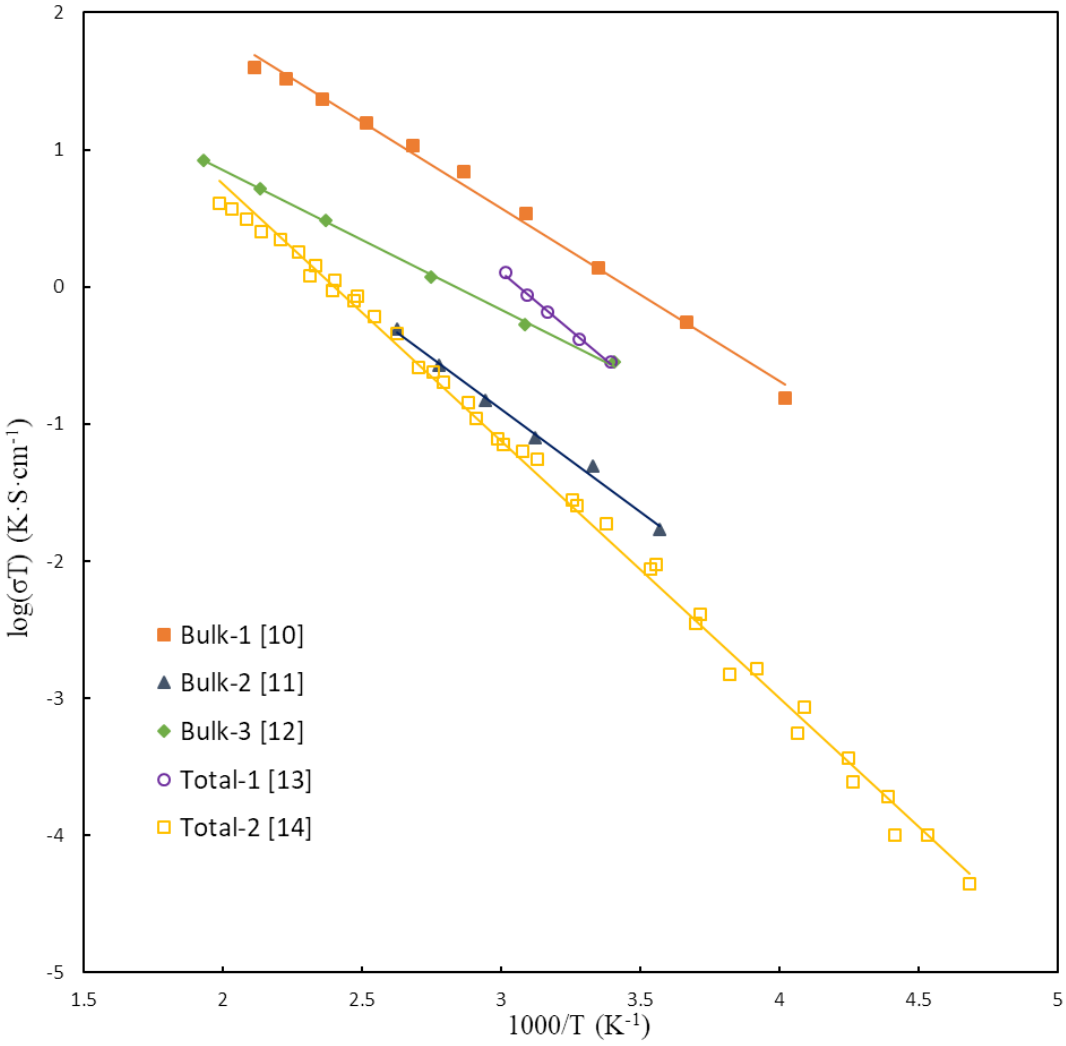

Figure 8. Arrhenius plots of LATP conductivity.

Chapter 3

Experiments

3.1 EIS Measurement for β-Alumina $Na_2O \cdot 11Al_2O_3$

3.1.1 Preparation

The β-Alumina samples were purchased from Ionotec Ltd. The geometrical shape of the sample is disk-like with 0.1 cm of thickness and 2 cm of diameter. The samples are preserved in a vacuum glove box before the experiment. The sample was sputtered with gold on the top and bottom as two electrodes. The edge of the sample was ground to remove any gold that may have deposited and might provide a conductive path between the electrodes. The geometry of β-alumina sample is shown in Figure 9.

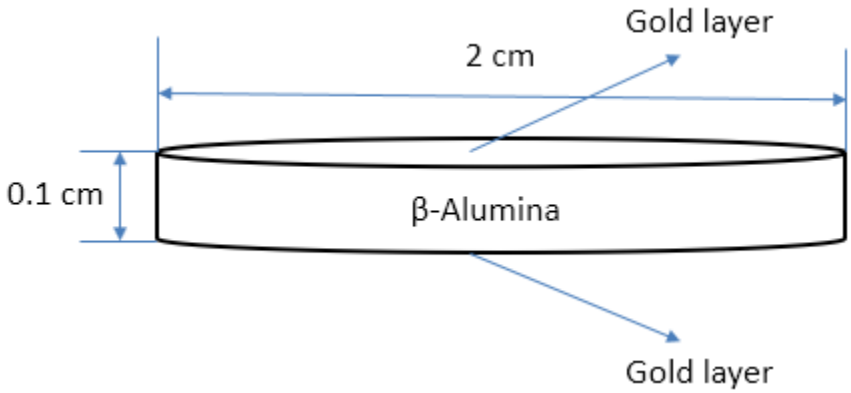

Figure 9. Geometry of β-alumina sample.

3.1.2 Impedance Test

A device made of ceramic was used to fix the sample in the furnace. There are two hollow ceramic tubes with a fastener. The sketch of the device is shown in Figure 10. The picture of the device is shown in Figure 11.

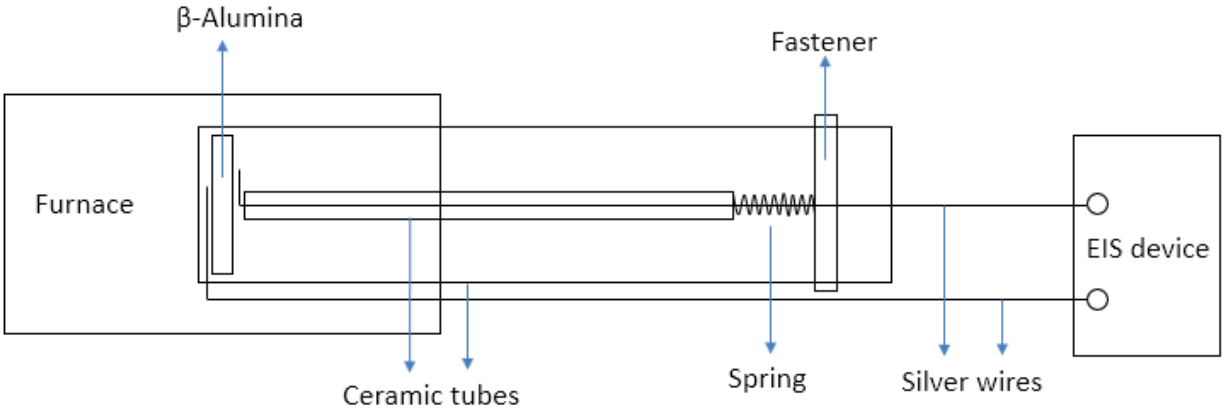

Figure 10. Impedance test system of β-alumina.

Figure 11. Picture of the equipment.

First, the sample with gold coating was placed at the left side of the large tube with one side containing a silver wire beneath it. Another wire goes across the small tube with one side extending out of the tube. Then, the small tube with wire was pressed toward the sample to make the sample and two sides of wires contact tightly. The fastener was used to fix the position of the two tubes, so the sample has good contact with the two wires. The spring between the fastener

and tube was used to provide a continuous force. Then, the left side of the large tube was put into the middle of the furnace. The other sides of the two wires were connected to the EIS device.

For the β-Alumina samples, the impedance measurements were conducted at 20℃, 50℃, 100℃, 150℃, 200℃, 250℃, 300℃ and 350℃ respectively with a frequency range of 32MHz-0.5Hz.

With the sample in the furnace, the furnace temperature was set at 20℃. There was a 30-minute wait before the impedance test to make the temperature of the sample stable. Then, the impedance test was performed on the computer, and the original test results were saved. Next, the temperature was increased to 50℃, and identically, another 30-minute interval wait before the impedance test. The same process was performed for the rest of the temperatures. After the impedance test, the original results were managed and output by Z-view software. An equivalent circuit was built to simulate the electrical property of the sample to get the numerical impedance of the β-Alumina sample.

3.2 EIS Measurement for NASICON Type $Li_{1.3}Al_{0.3}Ti_{1.7}(PO_4)_3$

3.2.1 Preparation

$Li_{1.3}Al_{0.3}Ti_{1.7}(PO_4)_3$ samples were prepared by the co-precipitation method. The flowcharts are shown in Figure 12.

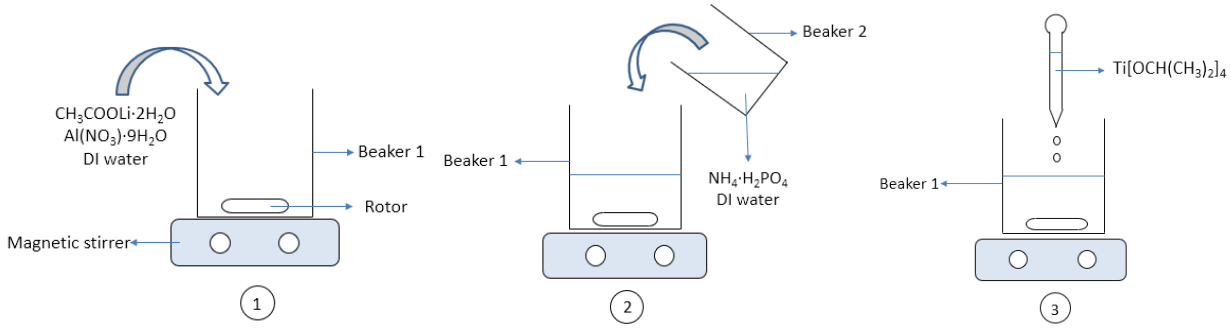

Figure 12. Preparation of $Li_{1.3}Al_{0.3}Ti_{1.7}(PO_4)_3$.

7.85g of $CH_3COOLi \cdot 2H_2O$ and 7.5g of $Al(NO_3) \cdot 9H_2O$ were taken into beaker 1. A moderate amount of deionized water was added into beaker 1 to dissolve the compounds. A glass rod was used to stir the solution until the solutes fully dissolved and mixed. Then a magnetic rotor was put into beaker 1, and it was then placed on a magnetic stirrer and the stirring continued. 17.25g of $NH_4 \cdot H_2PO_4$ was taken into beaker 2 and a moderate amount of deionized water was added to dissolve it. A glass rod was used to stir the solution, and the solution was slowly poured into beaker 1. Then, 23.65ml of $Ti[OCH(CH_3)_2]_4$ was slowly dripped into beaker 1. Beaker 1 was then covered with dust free tissue. The heater of the magnetic stirrer was turned on at a low temperature. The solution became colloidal after around 24 hours. Then, beaker 1 was placed in the oven to making the colloid harder.

The colloid was then placed into a crucible. The crucible was then placed into the middle of a furnace with air circulating. The sintering process was performed at 330℃ with a 2-hour hold, and then, the temperature was increased to 850℃ with a 2-hour hold. The colloid became powdery after the sintering, and then, the powder was pressed into wafer samples.

The pressed samples were then placed into the furnace again. The heat controller was set up to slowly go up to 900℃. Sintering samples were prepared at 6 hours and 14 hours. After the sintering, the samples were placed in a drying bottle for impedance test.

The X-ray diffraction patterns of LATP samples with 6 hours and 14 hours sintering time compared with the standard pattern 35-0754 $LiTi_2(PO_4)_3$ are shown in Figure 13.

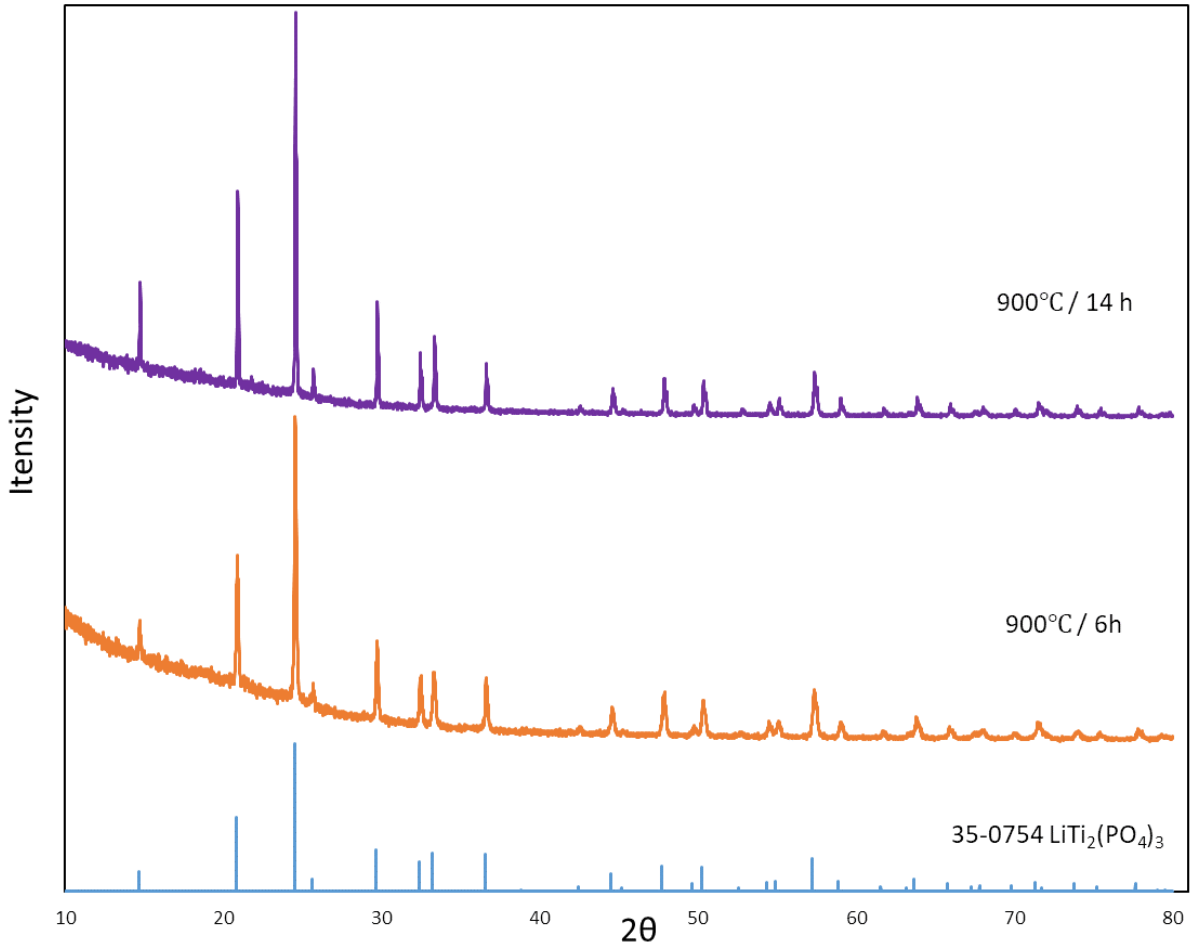

Figure 13. X-ray diffraction patterns of LATP sintered at 900 ℃ for 6h and 14h.

3.2.2 Impedance Test

The LATP samples do not have enough strength to withstand the high force of the spring and fastener, so another apparatus was used for the impedance test. The wafer sample was coated with silver paste on both sides as electrodes with silver wires attached to each side. The lateral side was ground to remove silver paste which may shortcut the sample. Both wires were covered by hollow ceramic tube to prevent the two wires from contacting. The sketch of the system is shown in Figure 14. The picture of the equipment is shown in Figure 15.

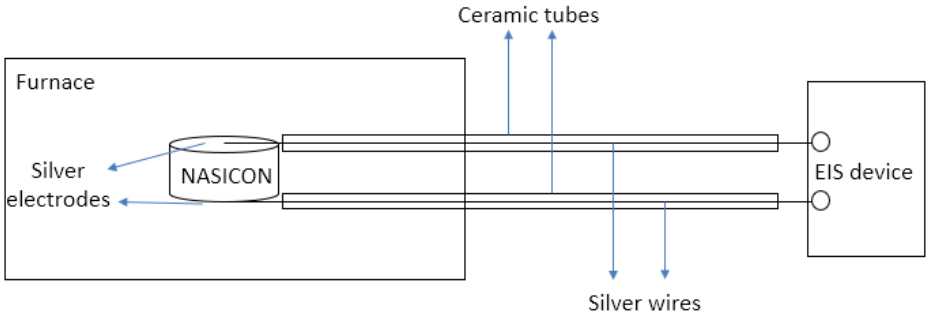

Figure 14. Impedance test system of LATP.

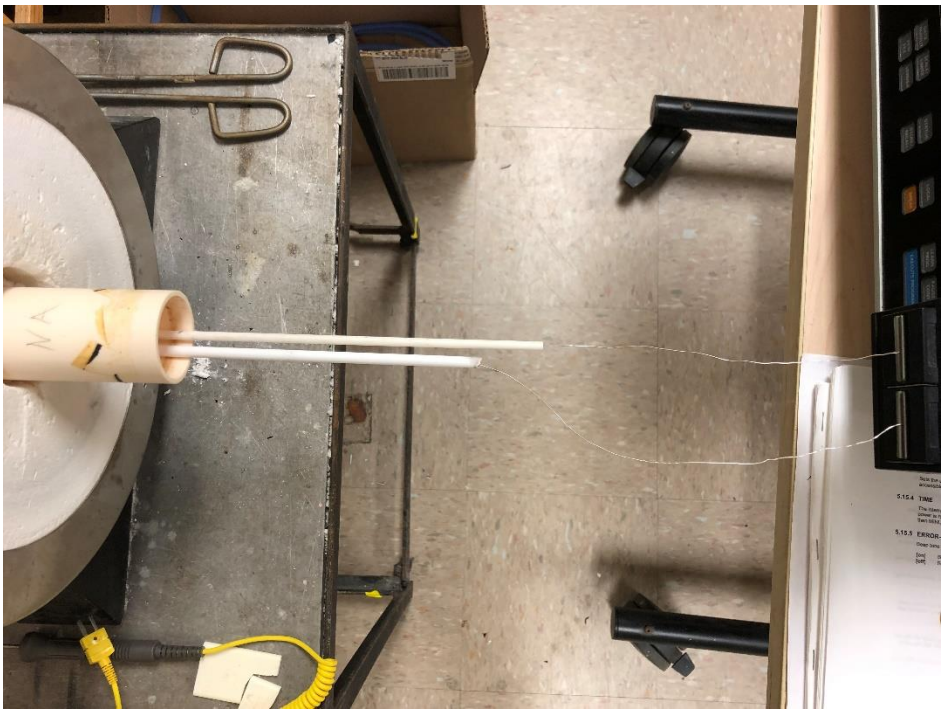

Figure 15. Picture of the impedance test system of LATP.

Usually, the liquid silver paste needs 2 hours to totally solidify. After 2 hours of solidification, the sample was put into the middle of the furnace. The right sides of the two wires were connected to the impedance test device.

For $Li_{1.3}Al_{0.3}Ti_{1.7}(PO_4)_3$, the impedance measurements were performed at 20℃, 40℃, 60℃, 80℃, and 100℃ respectively with a frequency range of 32MHz-0.5Hz.

The measurement process was similar to that used for the β-alumina samples. There needs to be a 30-minute interval before the impedance test at each of the temperatures. The original results were analyzed using Z-view software. The equivalent circuit of the β-Alumina sample can also be used on the $Li_{1.3}Al_{0.3}Ti_{1.7}(PO_4)_3$ to simulate the electrical property.

Chapter 4

Results and Discussion

4.1 Micromodel of Electrolyte-electrode System

A micromodel of solid electrolyte assembled with the electrode system was built to better understand ion migration pathways and influence factors of electrode system during EIS measurement. The micromodel of the system is shown in Figure 16. [2]

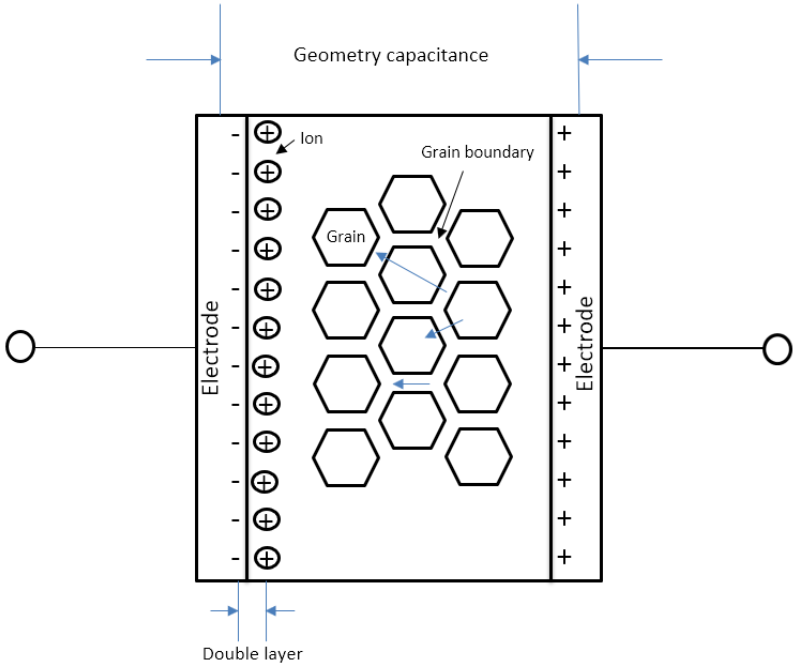

Figure 16. Micromodel of electrolyte and electrode system.

There are three pathways for ions to migrate among grains. Ions may pass through a grain from one side to another. The grain has resistance on ions' migration which is bulk resistance (R_b). Also, due to the potential difference at both sides of the grain, it may show a capacitor

behavior (C_b). These two behaviors occur simultaneously. Thus, the bulk resistor and the bulk capacitor should be in parallel as shown in Figure 17.

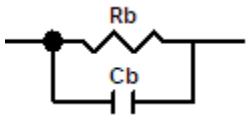

Figure 17. Equivalent circuit model for grain.

Ions may pass along grain boundaries which produces grain boundary resistance (R_{gb}). Also, ions may pass through grain boundary from one grain to another adjacent grain. Due to the potential difference between the two sides of the grain boundary, a capacitive behavior (C_{gb}) shows up. These two behaviors occur simultaneously. Thus, the grain resistor and the grain capacitor should be in parallel as shown in Figure 18.

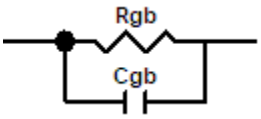

Figure 18. Equivalent circuit model for grain boundary.

Ions could go along a grain boundary or pass through it, then pass through a grain. For ceramic materials, the grain boundary resistance is much larger than the bulk resistance. As ions go along the grain boundary with high resistance, they prefer to go through a grain with lower resistance instead of going along the grain boundary all the way. Therefore, ions will go along the grain boundary, then pass through it into a nearby grain. After ions pass through the grain, they will again go along the grain boundary and then pass through it into another grain. Thus, the equivalent circuit of grain and grain boundary should be in series as shown in Figure 19.

Figure 19. Equivalent circuit model for grain and grain boundary.

A double layer will be generated when a layer of electrons exists in the surface of the electrode and a layer of ions exists adjacent to it. The ions could not transfer into the electrode if an ion-blocking electrode is used. A capacitive behavior (C_{dl}) shows up due to the potential difference between the two layers. Obviously, the double layer is in series with the electrolyte that contains grains and grain boundaries. The equivalent circuit model is shown in Figure 20.

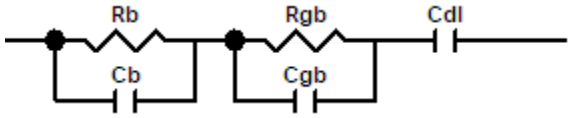

Figure 20. Equivalent circuit model for double layer.

Geometry capacitance (C_{geo}) is due to the two parallel metallic electrodes under high-frequency AC. The value of this capacitance is usually very small. The two electrodes act across the electrolyte, and they are nested structured with electrolyte. Thus, the geometry capacitor should be in parallel with the model of the electrolyte. This structure is called “Debye circuit”. [15] The equivalent circuit model of geometry capacitance is shown in Figure 21.

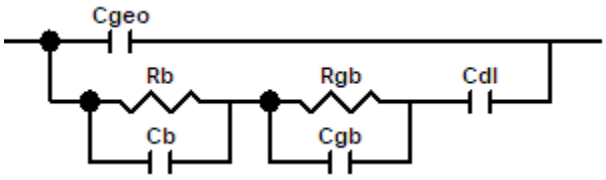

Figure 21. Equivalent circuit for geometry capacitor.

In the consideration of resistance and inductance of wires, they are in series with the electrodes and electrolyte. The equivalent circuit model of the whole electrode-electrolyte system is shown in Figure 22.

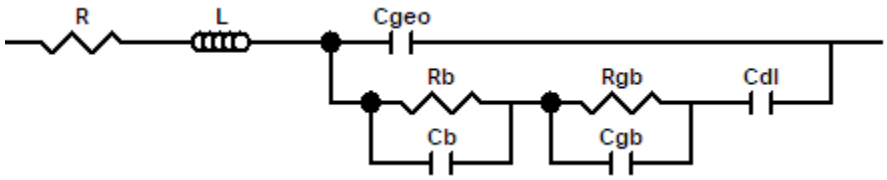

Figure 22. Equivalent circuit model for the electrode-electrolyte system.

4.2 Simplified Equivalent Circuit

In the practical experiment, an ideal capacitance (C) is usually replaced by a constant phase element (CPE) due to the dispersion effect discussed in chapter 1.3. Some circuit components can be removed depending on the complex plan and the fitting data to make the fitting process easier. Here, two circuit components, system resistance (R1) and bulk capacitance (C_b), could be removed. The simplified equivalent circuit is shown in Figure 23.

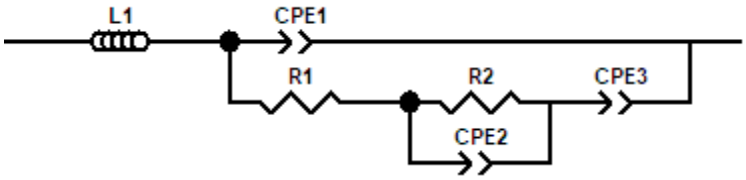

Figure 23. Simplified equivalent circuit.

The system resistance contains the resistance of two silver wires and two metallic electrodes. A multimeter was used to measure the resistance of the two pairs of wire-electrodes on both sides of the electrolyte after the system was set up properly. The total system resistance ranges from 0 to 1Ω. The system resistance is a very small value when compared with the

electrolyte resistance. Thus, in order to make the model simpler and the fitting process easier, the system resistance (R1) was removed.

In practical experiments, it is difficult for grains to show capacitor behavior because the geometry of a grain may be an irregular polygon or ellipse and does not have two parallel sides. Another reason for it is difficult for grains to show capacitor behavior is that the bulk capacitive circle may show up in a frequency region, which is too high and exceeds the frequency limit of the equipment. [16] There is no semicircle at high frequency from the impedance spectrum, which means there is no capacitive property, so the bulk capacitance was removed.

4.3 β-Alumina $Na_2O \cdot 11Al_2O_3$

The β-Alumina solid electrolyte was tested by EIS at 20℃, 50℃, 100℃, 150℃, 200℃, 250℃, 300℃ and 350℃ respectively. The EIS test results and Z-view fitting results are shown in Figure 24-31.

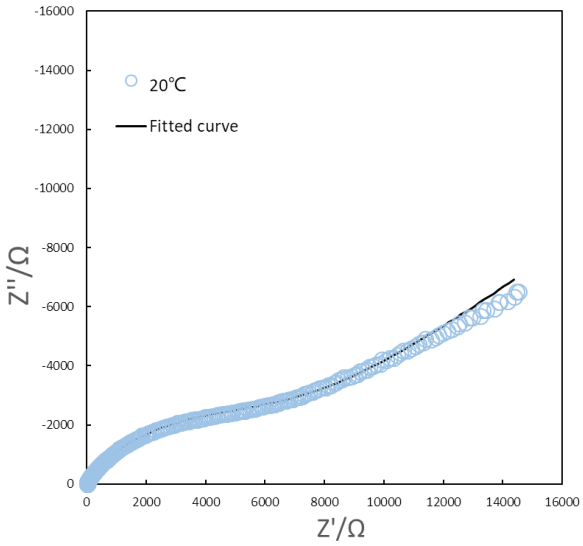

Figure 24. EIS test results and fitting results of β-alumina at 20℃.

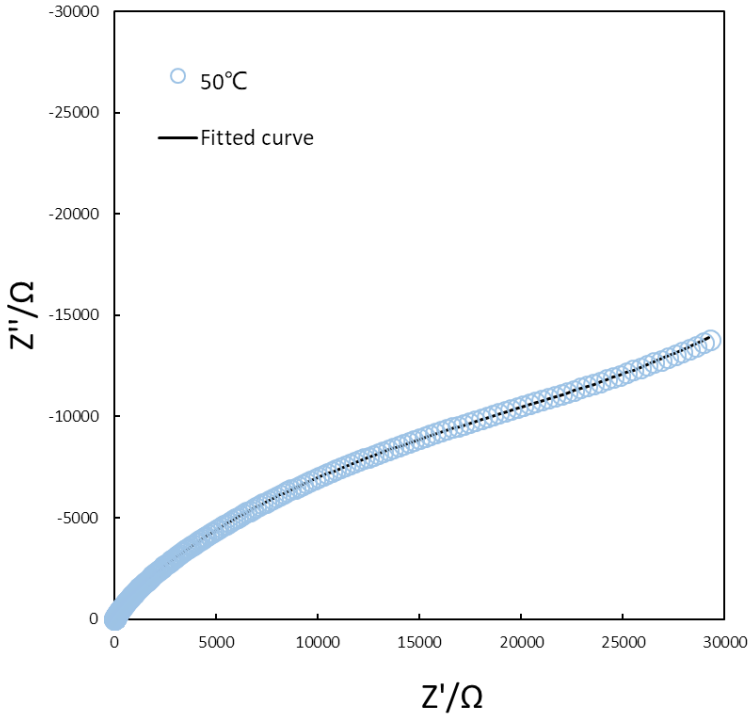

Figure 25. EIS test results and fitting results of β-alumina at 50℃.

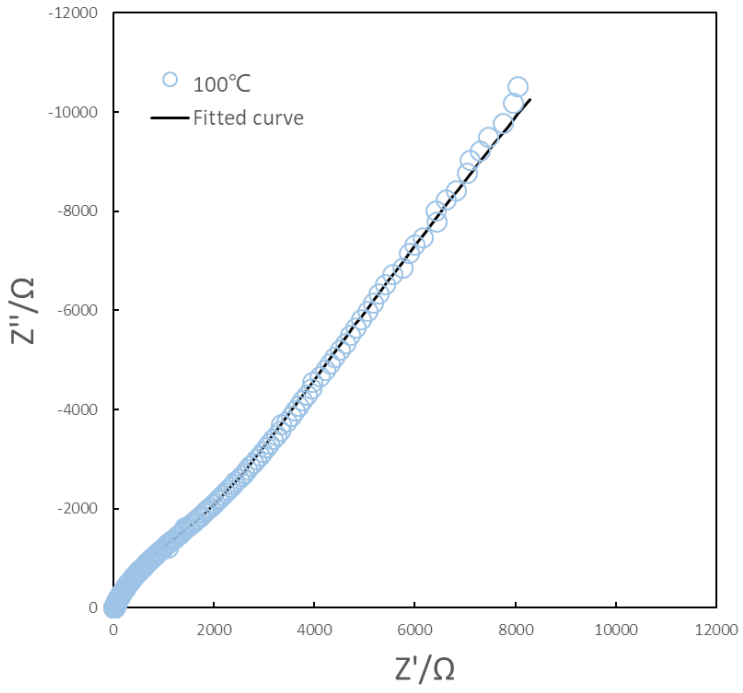

Figure 26. EIS test results and fitting results of β-alumina at 100℃.

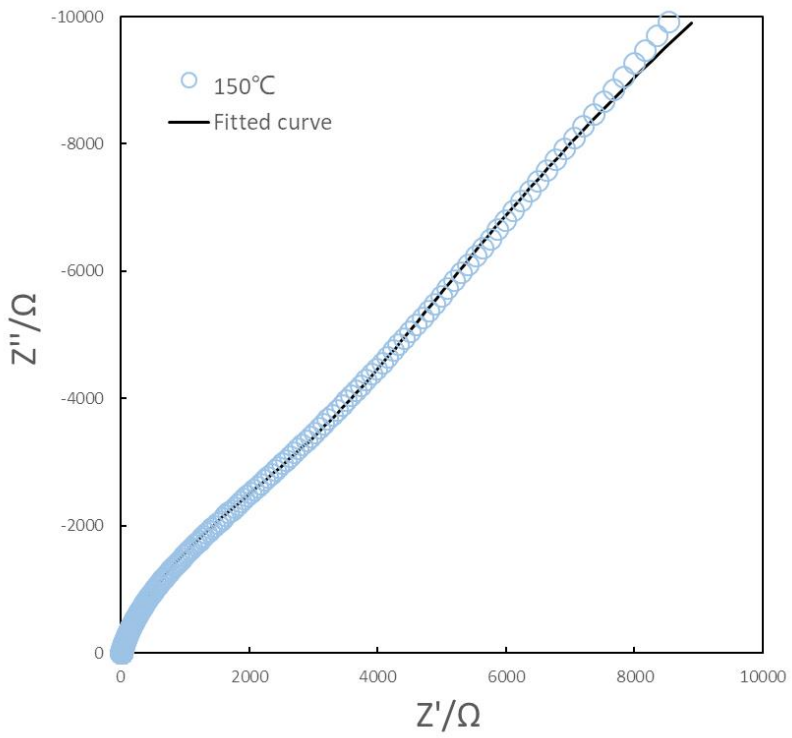

Figure 27. EIS test results and fitting results of β-alumina at 150℃.

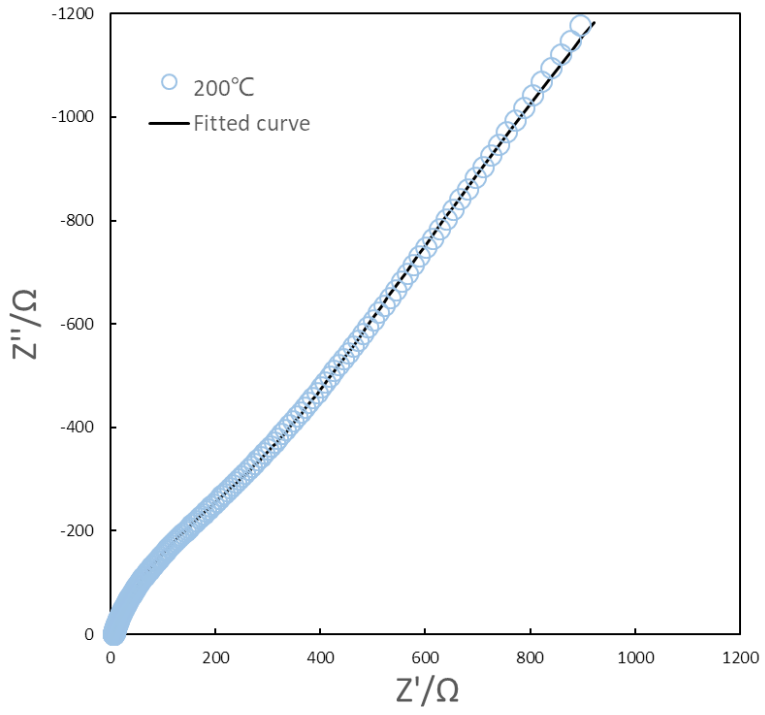

Figure 28. EIS test results and fitting results of β-alumina at 200℃.

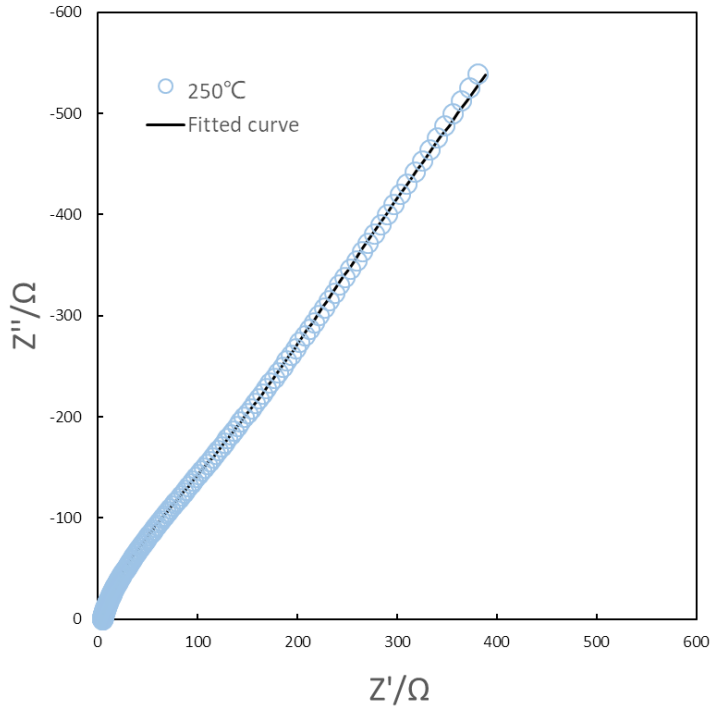

Figure 29. EIS test results and fitting results of β-alumina at 250℃.

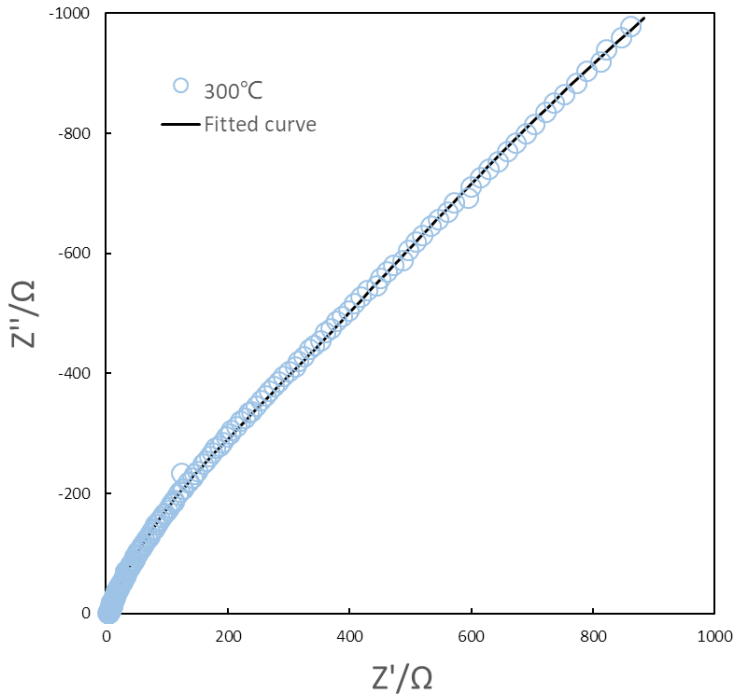

Figure 30. EIS test results and fitting results of β-alumina at 300℃.

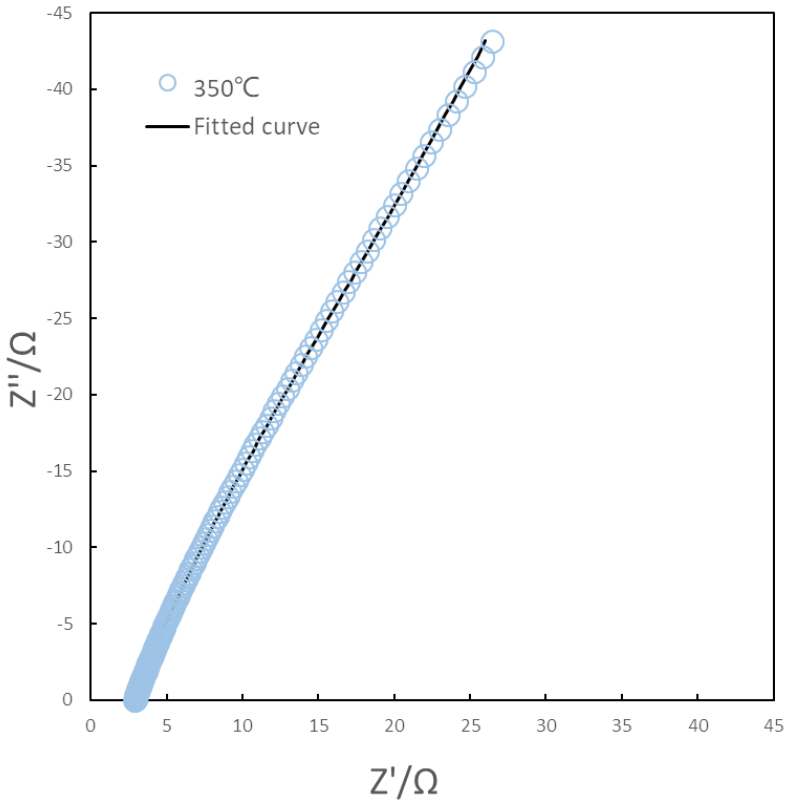

Figure 31. EIS test results and fitting results of β-alumina at 350℃.

In the Nyquist plots, which are also the impedance complex plots, the frequency goes down from the left side of the Z' axis to the right side of the Z' axis, which means the highest frequency point located at the far left and the lowest frequency point located at the rightmost. As the frequency decreases, both impedance of the real part and the imaginary part increase.

At high frequency, the plot has an intercept with the Z' axis. The reason for this intercept is that components CPE2 and CPE3 are short cut due to the high-frequency AC current according to equation (4.3.1), where Xc is capacitive reactance, f is frequency, and C is capacitance.

$$Xc = \frac{1}{2\pi fC} \qquad (4.3.1)$$

When frequency (f) is extremely high, capacitive reactance (Xc) for CPE2 and CPE3 is extremely low, so CPE2 and CPE3 can be considered as wires. The currents go through elements L1, R1, CPE2, and CPE3.

At medium frequency range, there is a depressed semicircle. As the frequency (f) decreases, the capacitive reactance (Xc) of CPE2 and CPE3 increases, so they can no longer be considered as wires. The currents go through L1, R1, R2, CPE2, and CPE3. The inductive impedance of L1 decreases as frequency decreases.

At low frequency, as frequency keeps decreasing, the capacitive reactance of CPE2 and CPE3 keeps increasing, so the total impedance of the system keeps increasing.

The geometry capacitor CPE1's capacitive reactance (Xc) is very large due to the small capacitance (C). Small currents may go through CPE1 at the high and medium frequencies, but there was no current goes through at low frequency.

The Bode plots show the relationship between the value of total impedance and frequency and the value of phase angle and frequency. For both Nyquist plots and Bode plots, the fitting plots show high coincidence with the EIS results. The Bode plots and fitting results are shown in the appendix.

According to the Z-view fitting results, total resistance (R), bulk conductivity (σ1), grain boundary conductivity (σ2), and total conductivity (σ) were calculated using equations:

$$R=R1+R2 \qquad (4.3.2)$$

$$\sigma = \frac{t}{AR} \qquad (4.3.3)$$

Where t is the thickness of the electrolyte, t=0.11 cm. A is the electrolyte-electrode contact area, A=3.14 cm^2. R is the total resistance. Table 1 shows the resistance and conductivity of the β-Alumina at different temperatures.

Table 1. Resistance and conductivity of β-alumina

t/℃	R1/Ω	R2/Ω	R/Ω	σ1/Scm-1	σ2/Scm-1	σ/Scm-1
20	28.8	7237	7265.8	1.2E-03	4.8E-06	4.8E-06
50	12.1	52387	52399.1	2.9E-03	6.7E-07	6.7E-07
100	9.2	1244	1253.2	3.8E-03	2.8E-05	2.8E-05
150	7.2	3706	3713.2	4.9E-03	9.4E-06	9.4E-06
200	6.9	516.7	523.6	5.1E-03	6.8E-05	6.7E-05
250	5.8	281.7	287.5	6.0E-03	1.2E-04	1.2E-04
300	3.1	160.8	163.9	1.1E-02	2.2E-04	2.1E-04
350	3.0	66.1	69.1	1.2-02	5.3E-04	5.1E-04

Arrhenius plots were obtained according to the value of σ1, σ2, and temperature. The Arrhenius plots of σ1 and σ2 are shown in Figure 32 and Figure 33. Activation energies of both were calculated by equations: [17]

$$\sigma = \frac{C}{T}\exp(-\frac{Ea}{KT}) \qquad (4.3.4)$$

$$\mathrm{Ln}(\sigma T) = -\frac{Ea}{1000K}\frac{1000}{T} + \mathrm{Ln}C \qquad (4.3.5)$$

where σ is conductivity, C is constant about the material property, Ea is activation energy, k is Boltzmann Constant (k=8.61733x10^{-5}eV/K), and T is temperature.

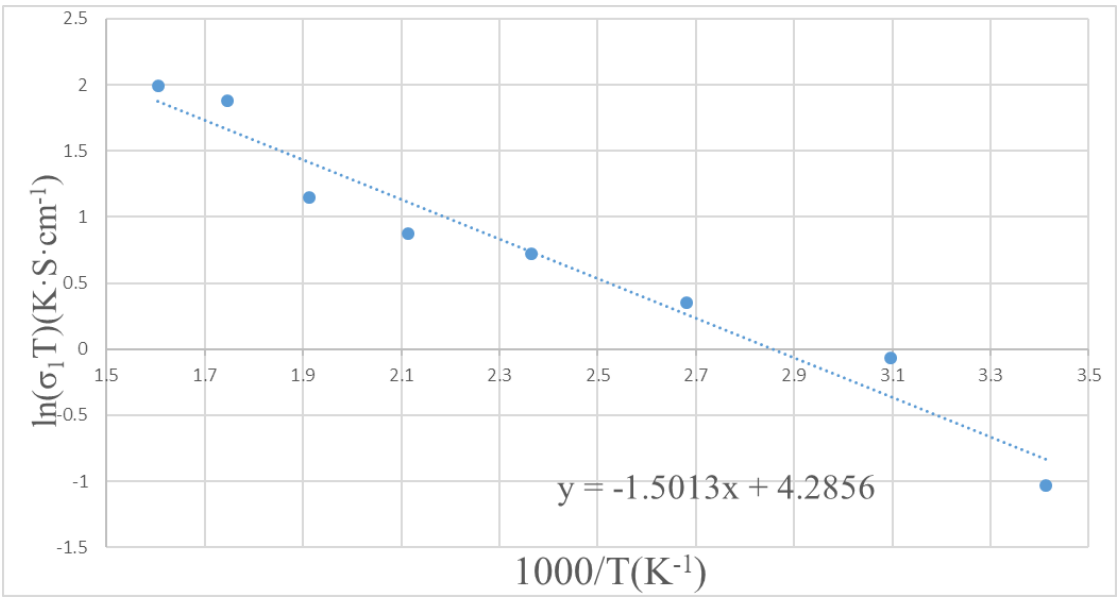

Figure 32. Arrhenius plot of σ1.

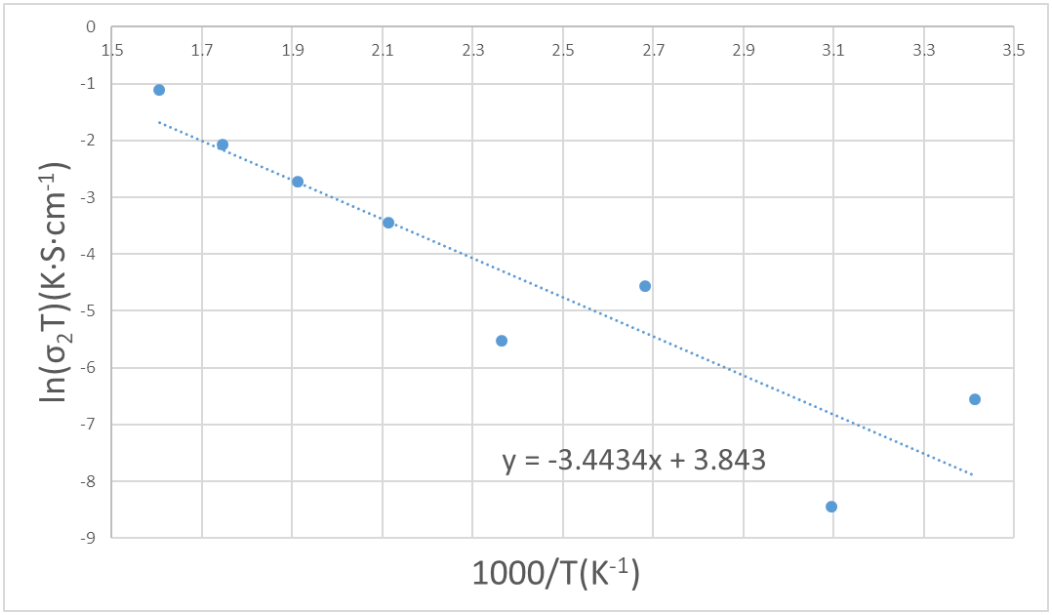

Figure 33. Arrhenius plot of σ2.

The bulk activation energy for σ1 is Ea_1=0.13 eV. The grain boundary activation energy for σ2 is Ea_2=0.30 eV. These two activation energies are consistent with the results reported by A Hooper [6] that Ea_{bulk}=0.15 eV, Ea_{total}=0.27 eV. Thus, for the β-Alumina $Na_2O·11Al_2O_3$, the

resistance (R1) could be associated with the bulk resistance, and the resistance (R2) could be associated with the grain boundary resistance.

The Arrhenius plots are compared with the results of other researchers and shown in Figure 34.

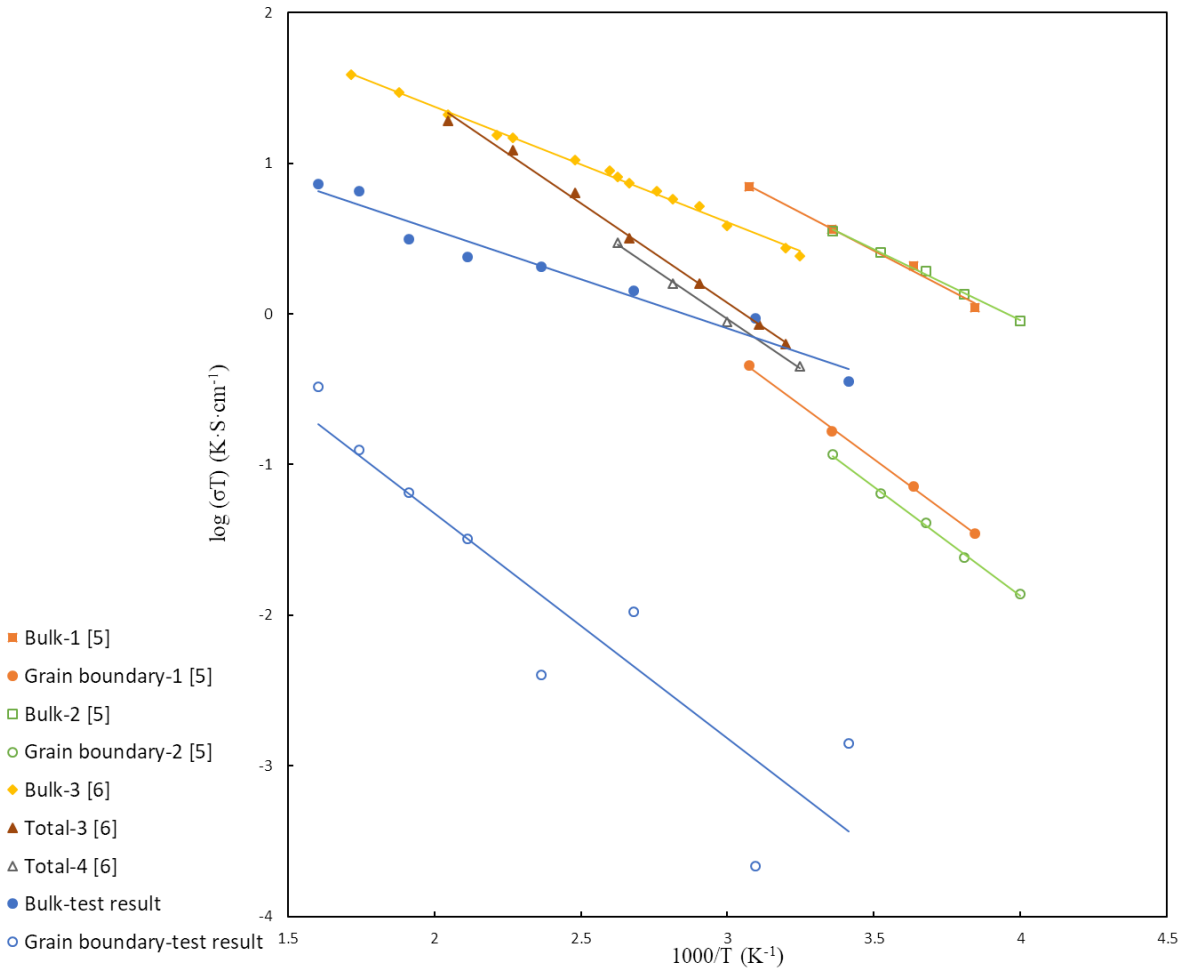

Figure 34. Arrhenius plot of β-alumina compared to other researchers' studies.

The test result for bulk conductivity is an order of magnitude smaller than the results of other researchers' studies. Grain boundary conductivity is about two orders of magnitude smaller than the results of other researchers' studies, and the conductivity at low temperatures is unstable. A possible reason for the unstable conductivity is the absorption of water during the

sample preparation and test in the air. Will [18] reported that the bulk conductivity of β-alumina decreases from $2.27x10^{-3}$ S/cm for a dry disk to $1.89x10^{-3}$ S/cm after long-term exposure to water vapor. The grain boundary conductivity decreases from $1.48x10^{-3}$ S/cm to $1.16x10^{-4}$ S/cm. Water decreases the conductivity of grain boundaries by more than an order of magnitude, and the decrease in grain conductivity is about 20%.

4.4 NASICON Type $Li_{1.3}Al_{0.3}Ti_{1.7}(PO_4)_3$ (LATP)

NASICON type solid electrolyte $Li_{1.3}Al_{0.3}Ti_{1.7}(PO_4)_3$ was tested by EIS at 20℃, 40℃, 60℃, 80℃, and 100℃ respectively. The EIS test results and Z-view fitting results are shown in Figure 35-39. The Bode plots and fitting results are shown in the appendix.

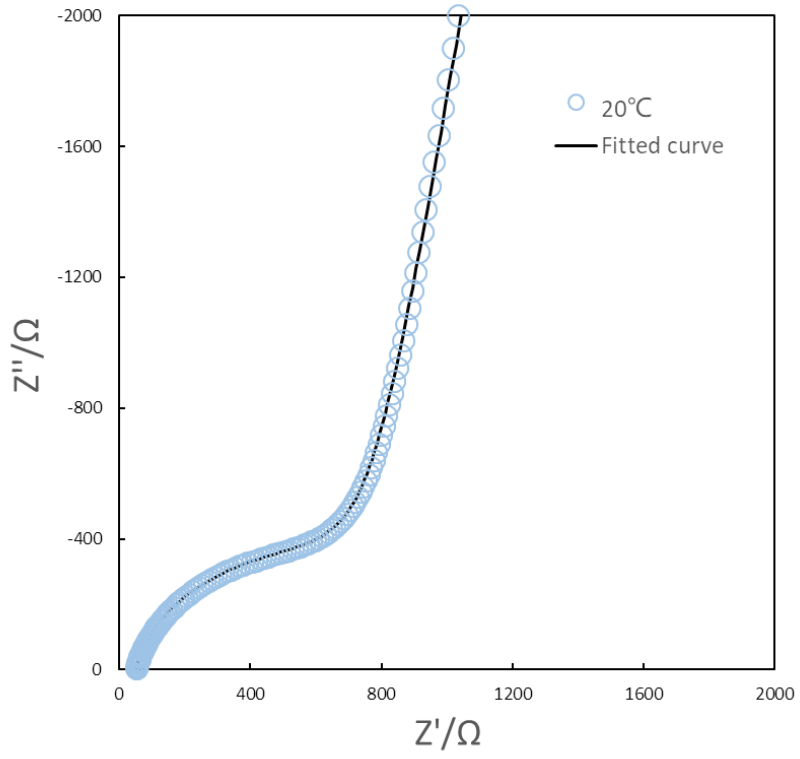

Figure 35. EIS test results and fitting results of $Li_{1.3}Al_{0.3}Ti_{1.7}(PO_4)_3$ at 20℃.

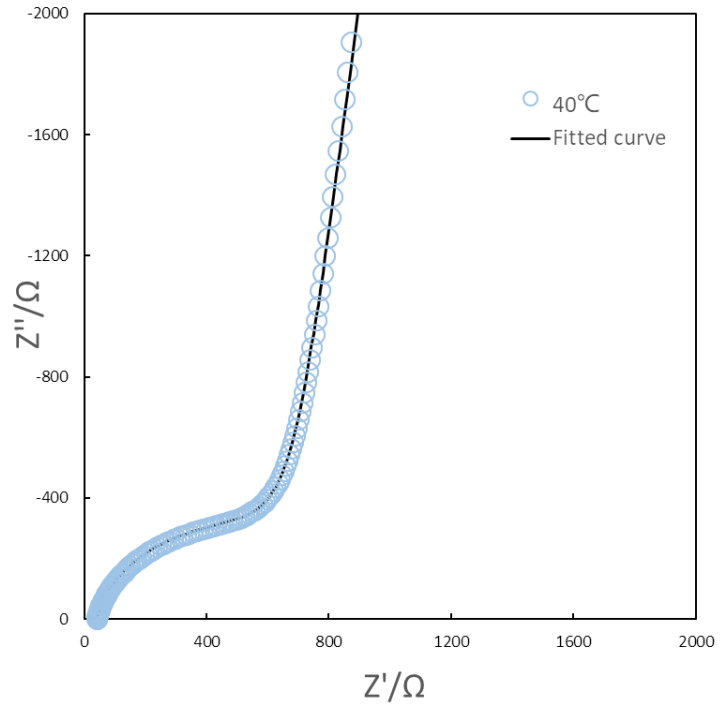

Figure 36. EIS test results and fitting results of $Li_{1.3}Al_{0.3}Ti_{1.7}(PO_4)_3$ at 40℃.

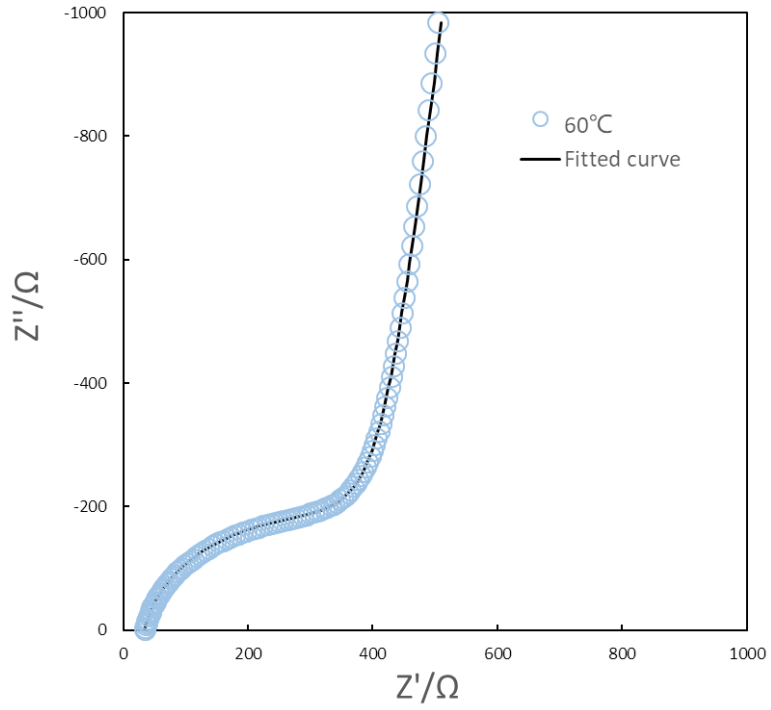

Figure 37. EIS test results and fitting results of $Li_{1.3}Al_{0.3}Ti_{1.7}(PO_4)_3$ at 60℃.

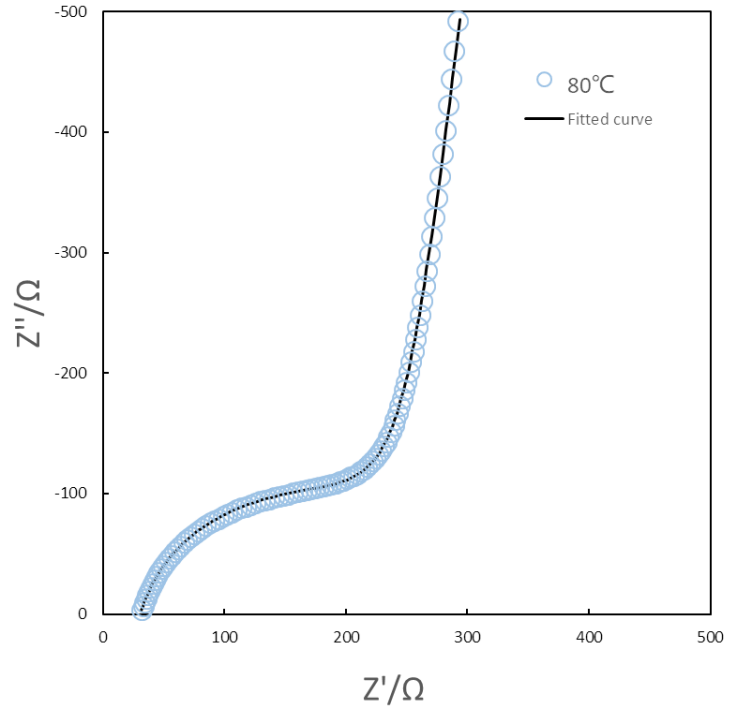

Figure 38. EIS test results and fitting results of $Li_{1.3}Al_{0.3}Ti_{1.7}(PO_4)_3$ at 80℃.

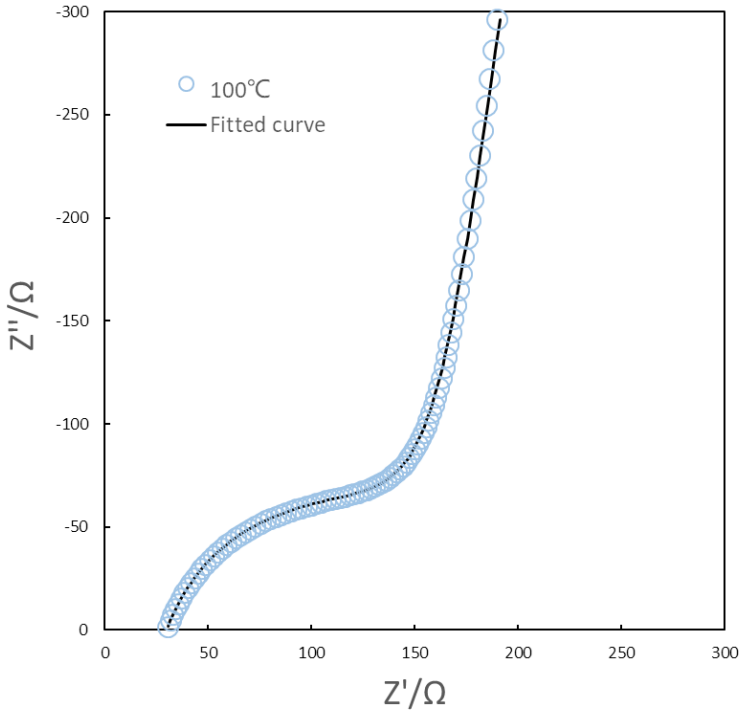

Figure 39. EIS test results and fitting results of $Li_{1.3}Al_{0.3}Ti_{1.7}(PO_4)_3$ at 100℃.

The overall impedance complex plots are similar to those of β-Alumina. An intercept with the real axis, a depressed semicircle, and a line are shown in each complex plot. At high frequency, the current breakdown the double layer capacitor and the grain boundary capacitor. The current goes through the bulk. At medium frequency, the current goes through the bulks, grain boundaries and goes along grain boundaries.

At low frequency, there is a line with curvature. The reason for this curve is the electrode polarization. [19-20] For the imaginary axis, as frequency keeps decreasing, the impedance of the double layer capacitor keeps increasing to infinity. For the real part, as frequency decreases, the impedance increases due to the polarization of the electrode. The electrode polarization is a phenomenon that charges aggregate at the electrode surface to obtain an electric balance. For this thesis, the blocking electrode was used so that the charges could not go through the electrode. When there are charges on one side of the electrode surface, these charges will cause a repulsive force to resist those charges that still in the electrolyte and continue coming to the electrode. This repulsive force causes an increase in impedance. And as the frequency becomes lower, the electrode polarization phenomenon is stronger. The impedance of the real part may have a higher increasing rate than the impedance of the imaginary part. Thus, a convex curve line is shown at a low frequency.

According to the Z-view fitting results, total resistance R, bulk conductivity σ1, grain boundary conductivity σ2, and total conductivity σ were calculated. Table 2 shows the resistance R1, R2, R and conductivity of each by using equation (4.3.2) and equation (4.3.3) where t=0.105 cm, and A=1.09 cm^2.

Table 2. Resistance and conductivity of $Li_{1.3}Al_{0.3}Ti_{1.7}(PO_4)_3$.

t/°C	R1/Ω	R2/Ω	R/Ω	σ1/Scm-1	σ2/Scm-1	σ/Scm-1
20	35.9	739.1	775.0	2.7E-03	1.3E-04	1.2E-04
40	23.4	662.5	685.9	4.1E-03	1.4E-04	1.4E-04
60	15.2	401.5	416.7	6.3E-03	2.4E-04	2.3E-04
80	9.0	244.9	254.0	1.1E-02	3.9E-04	3.8E-04
100	7.3	154.2	161.5	1.3E-02	6.2E-04	5.9E-04

From the table, R1 and R2 decrease as the temperature increases. The conductivity of both R1 and R2 increase. The Arrhenius plots were obtained according to σ1, σ2, and temperature. Arrhenius plots of σ1and σ2 were shown in Figure 40 and Figure 41.

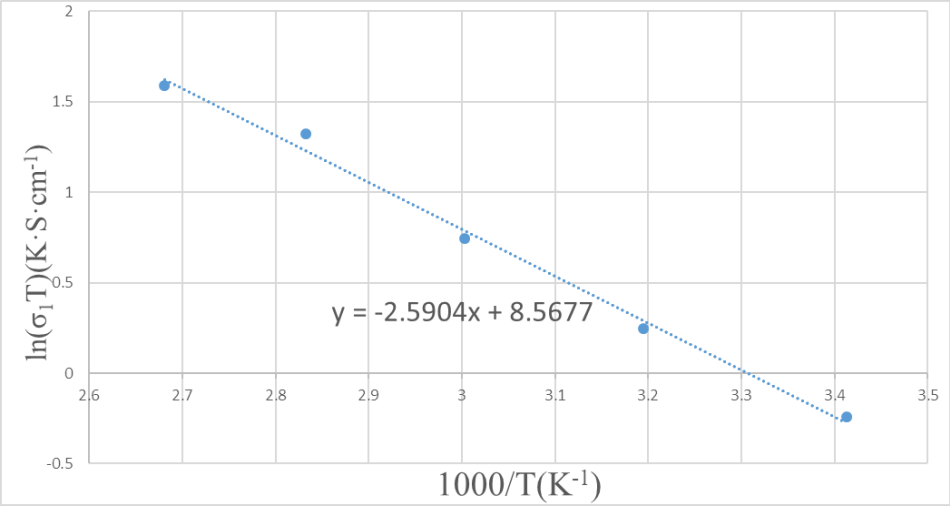

Figure 40. Arrhenius plot of σ1.

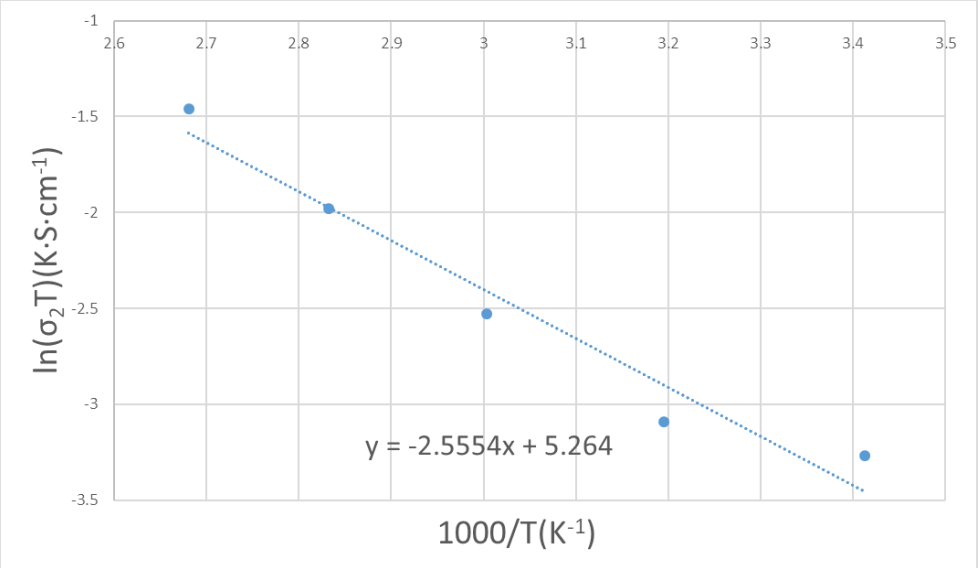

Figure 41. Arrhenius plot of σ2.

The activation energy was calculated by the equation (4.3.5). The bulk activation energy for σ1 is Ea_1=0.22 eV. The grain boundary activation energy for σ2 is Ea_2=0.22 eV. Both of these two activation energies are consistent with the results reported by N.V.Kosova et al's that Ea_{bulk}=0.23eV and Ea_{gb}=0.20eV. [14] They can be distinguished by comparing the conductivity of R1 and R2. It is known that for conductive ceramic materials, bulk resistance is much smaller than grain boundary resistance, which means the resistance is dominant by the grain boundary. Thus, for $Li_{1.3}Al_{0.3}Ti_{1.7}(PO_4)_3$, the resistance R1 could be associated with the bulk resistance, and the resistance R2 could be associated with the grain boundary resistance.

At 20℃, a relatively high bulk conductivity was obtained, $\sigma_{bulk}=2.7x10^{-3}$ S/cm was compared with H. Aono et al's [21] work $\sigma_{bulk}=3.0x10^{-3}$ S/cm. The total conductivity is $\sigma_{total}=1.2x10^{-4}$ S/cm which is lower than Ren et al's [22] report $\sigma_{total}=7x10^{-4}$ S/cm, but it is in the same order of magnitude.

The Arrhenius plots are also compared with the results of other researchers and shown in Figure 42.

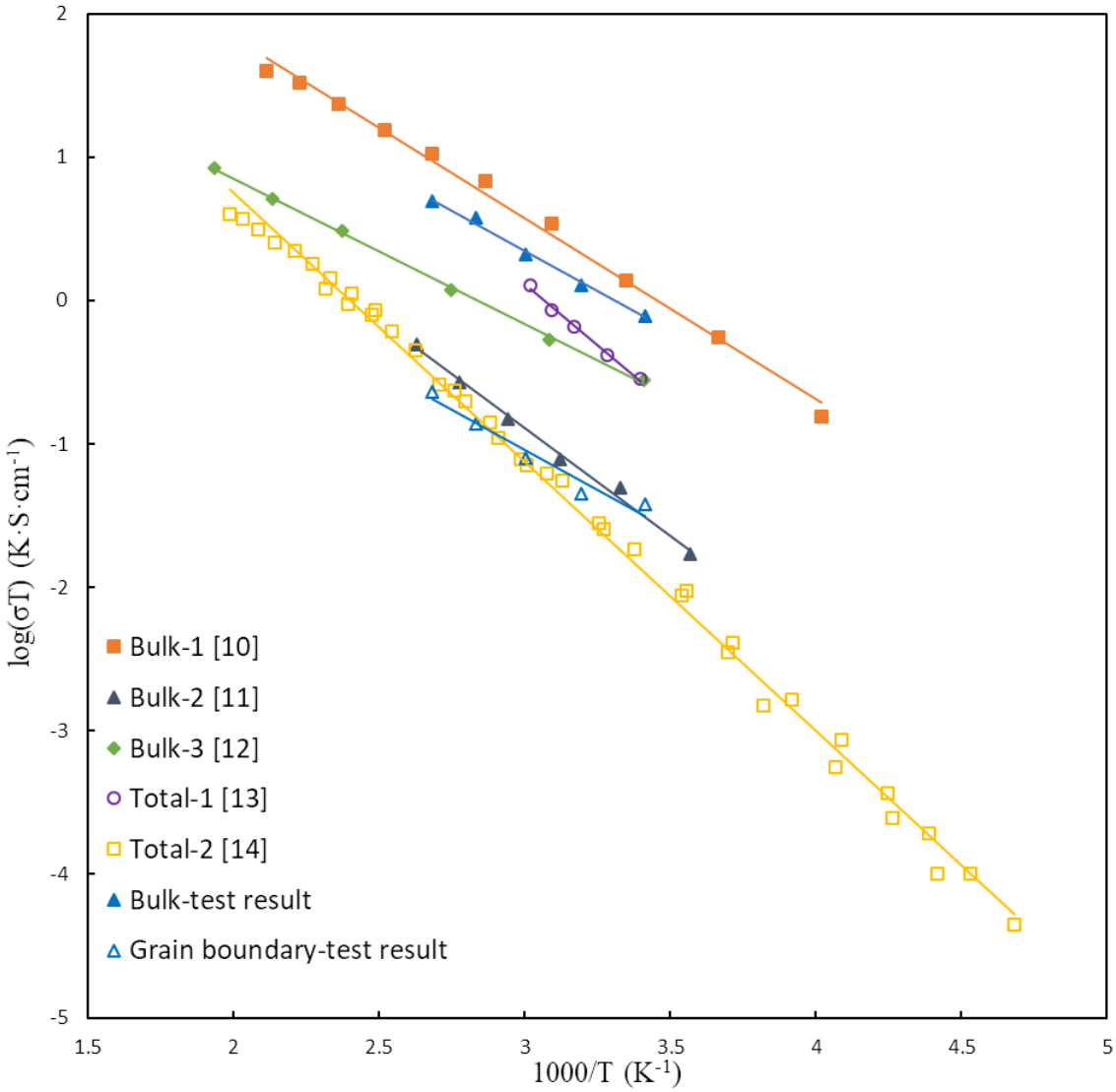

Figure 42. Arrhenius plot of LATP compared to other researchers' studies.

The Arrhenius plots of bulk and grain boundary conductivity are in the right range compared to the results of other researchers.

4.5 Fitting Results Compares with Simpler Model

The impedance plot fitted by the complex model was compared with the plot that fitted by the simpler model. The fitting results and data are shown in Figure 43-44.

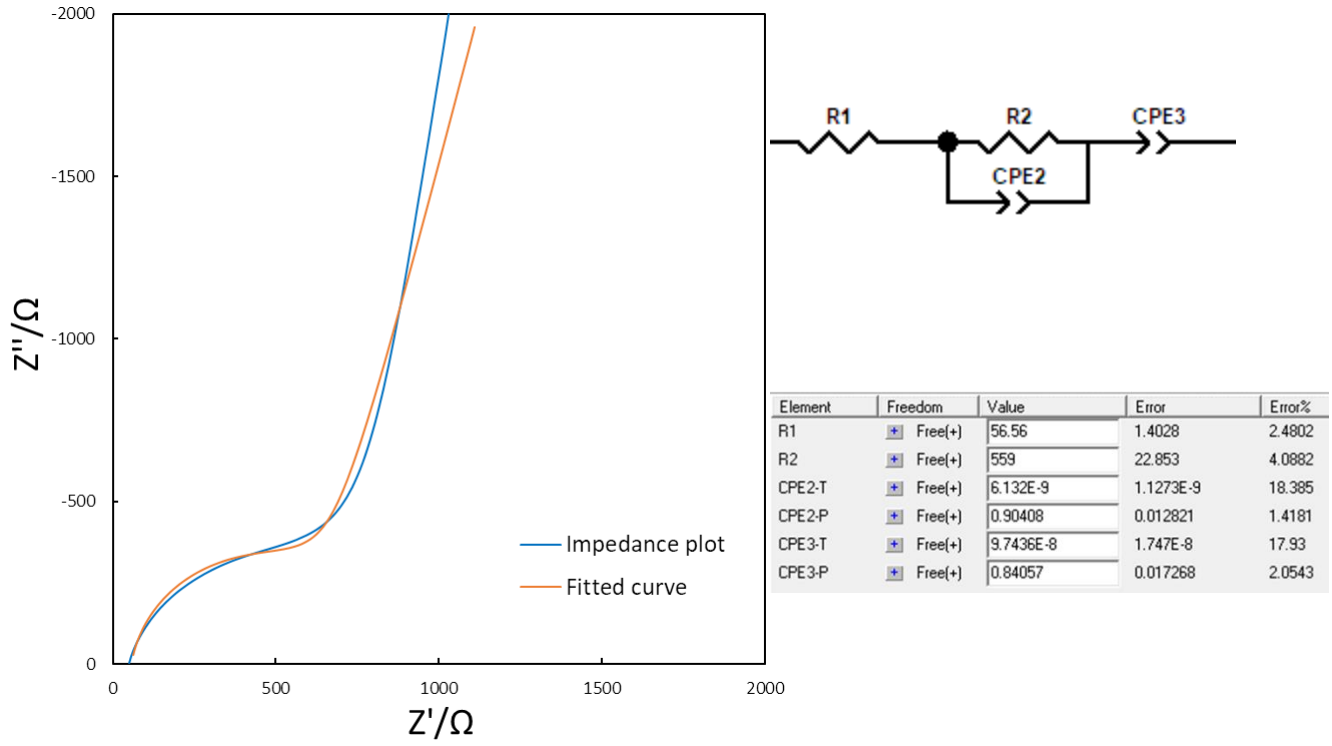

Element	Freedom	Value	Error	Error%
R1	Free(+)	56.56	1.4028	2.4802
R2	Free(+)	559	22.853	4.0882
CPE2-T	Free(+)	6.132E-9	1.1273E-9	18.385
CPE2-P	Free(+)	0.90408	0.012821	1.4181
CPE3-T	Free(+)	9.7436E-8	1.747E-8	17.93
CPE3-P	Free(+)	0.84057	0.017268	2.0543

Figure 43. Fitting results of LATP fitted by the simpler model.

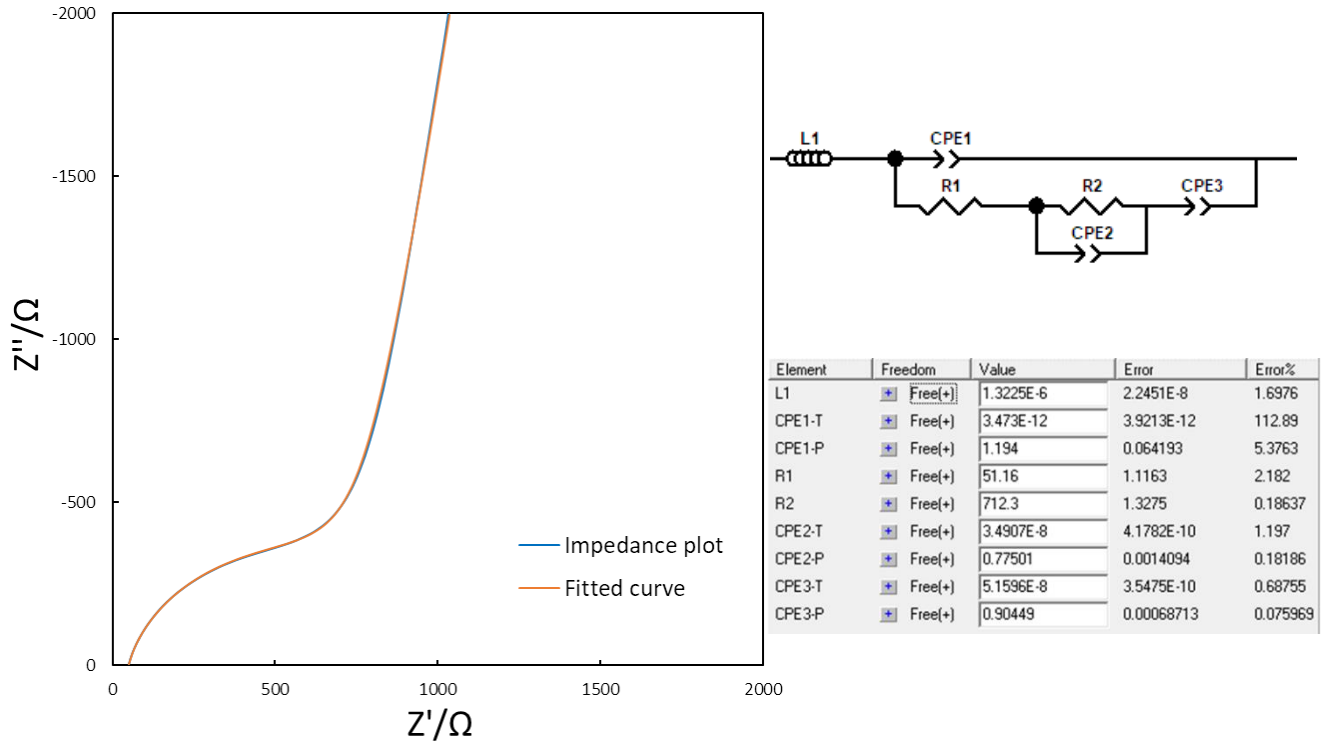

Element	Freedom	Value	Error	Error%
L1	Free(+)	1.3225E-6	2.2451E-8	1.6976
CPE1-T	Free(+)	3.473E-12	3.9213E-12	112.89
CPE1-P	Free(+)	1.194	0.064193	5.3763
R1	Free(+)	51.16	1.1163	2.182
R2	Free(+)	712.3	1.3275	0.18637
CPE2-T	Free(+)	3.4907E-8	4.1782E-10	1.197
CPE2-P	Free(+)	0.77501	0.0014094	0.18186
CPE3-T	Free(+)	5.1596E-8	3.5475E-10	0.68755
CPE3-P	Free(+)	0.90449	0.00068713	0.075969

Figure 44. Fitting results of LATP fitted by the complex model.

For the impedance plot fitted by the simpler model, there are some deviations between the impedance plot and the fitted curve. For the complex model, the impedance plot was perfectly fitted. The fitted curve has a high coincidence with the impedance plot. Thus, the complex model has a better fit than the simpler model.

4.6 Equivalent Circuit Model Verification

In order to show that the changes in the contributions to the different components change as predicted by the equivalent circuit model, the thickness and sintering time of the NASICON type $Li_{1.3}Al_{0.3}Ti_{1.7}(PO_4)_3$ samples were changed respectively.

4.6.1 Change in Thickness

The LATP sample of thickness with 0.45 cm was first tested. Then the same sample was ground to 0.23 cm and tested again. The Nyquist plots of the sample with both thicknesses are shown in Figure 45.

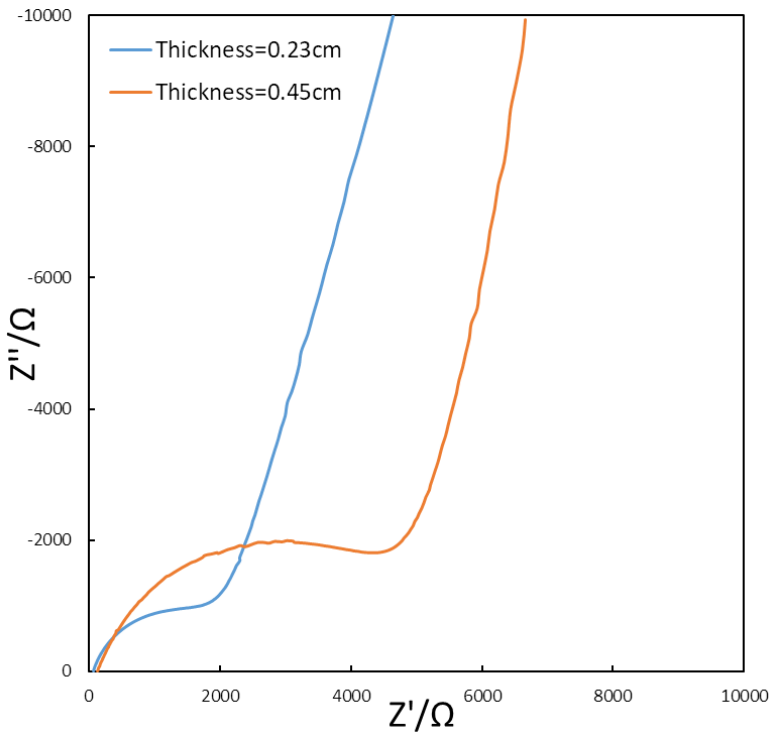

Figure 45. Nyquist plots of LATP with thickness 0.45cm and 0.23cm.

The fitting results were shown in Figure 46-47.

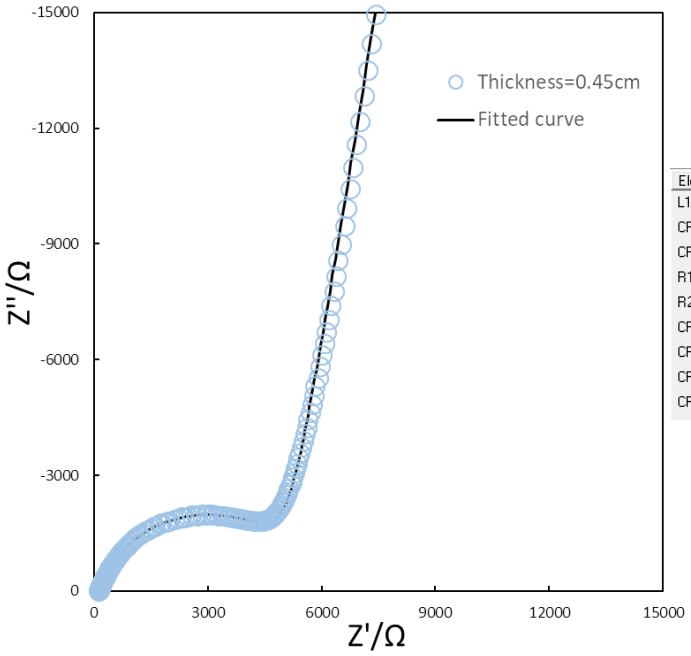

Element	Freedom	Value	Error	Error%
L1	Free(+)	1.1117E-6	2.5887E-8	2.3286
CPE1-T	Free(+)	8.642E-11	9.7429E-11	112.74
CPE1-P	Free(+)	0.93254	0.059143	6.3421
R1	Free(+)	206.8	10.85	5.2466
R2	Free(+)	4888	11.02	0.22545
CPE2-T	Free(+)	5.709E-9	3.5437E-10	6.2077
CPE2-P	Free(+)	0.7858	0.0019238	0.24482
CPE3-T	Free(+)	3.7682E-8	1.9021E-10	0.50478
CPE3-P	Free(+)	0.89885	0.00067225	0.07479

Figure 46. Fitting results of $Li_{1.3}Al_{0.3}Ti_{1.7}(PO_4)_3$ with thickness 0.45 cm at 40°C.

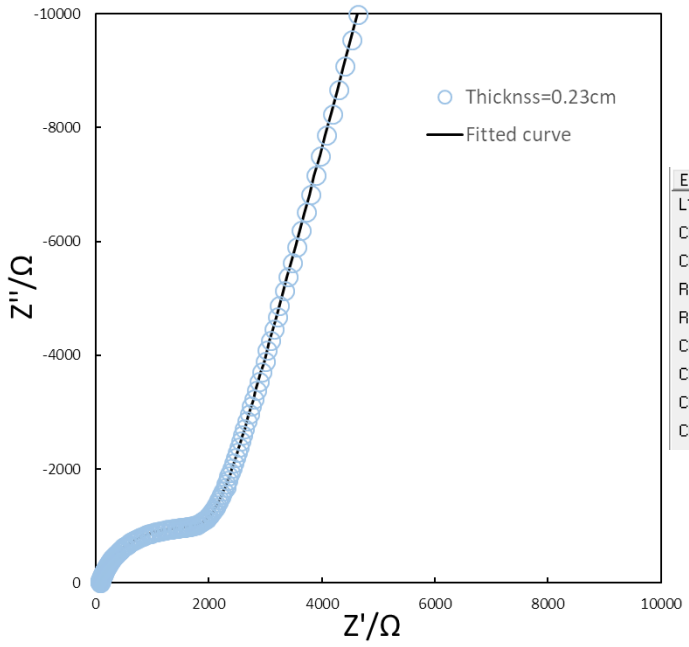

Element	Freedom	Value	Error	Error%
L1	Free(+)	1.1789E-6	1.6319E-8	1.3843
CPE1-T	Free(+)	2.216E-10	2.2173E-10	100.08
CPE1-P	Free(+)	0.93187	0.053452	5.736
R1	Free(+)	108	5.0046	4.6339
R2	Free(+)	1937	7.7413	0.39965
CPE2-T	Free(+)	1.0428E-8	7.5278E-10	7.2188
CPE2-P	Free(+)	0.80139	0.0022883	0.28554
CPE3-T	Free(+)	7.3623E-8	2.5156E-10	0.34169
CPE3-P	Free(+)	0.83541	0.00032588	0.039008

Figure 47. Fitting results of $Li_{1.3}Al_{0.3}Ti_{1.7}(PO_4)_3$ with thickness 0.23 cm at 40°C.

The fitting data are listed in Table 3.

Table 3. Fitting data of LATP with the thickness of 0.45 cm and 0.23 cm.

t/°C	Thickness/cm	R1/Ω	R2/Ω	L/H	CPE1/F	CPE2/F	CPE3/F
40	0.45	207	4888	1.1E-06	8.6E-11	5.7E-09	3.8E-08
40	0.23	108	1937	1.2E-06	2.2E-10	1.0E-08	7.4E-08

The NASICON type $Li_{1.3}Al_{0.3}Ti_{1.7}(PO_4)_3$ samples are powder-like with low density, and the density of the samples is not uniform. The samples also have a different degree of roughness of the sample surface after ground. The roughness of the sample surface causes deviations. The deviations are shown on the right side of Figure 46-47.

For bulk resistance R1, as the thickness decreases about half, the bulk resistance also decreases about half which is expected according to the equation:

$$R = \rho \frac{L}{A} \qquad (4.6.1.1)$$

where R is resistance, ρ is resistivity, L is length (thickness), A is cross-sectional area (no change for the same sample), and R is proportional to L.

The inductance (L) is caused by wire bending and not affected by thickness. Wire with more bending has much inductive effect and has larger values of L. Straighter wire has a less inductive effect and has smaller values of L. These two inductances have similar values.

The capacitor (CPE3) is the double layer capacitor that relates to the interface between the electrolyte and electrode, it is not affected by thickness. The roughness of the electrolyte-electrode interface causes some deviations. The values of CPE3 are similar for the two thickness samples which are expected.

For grain boundary resistance R2 and grain boundary capacitance CPE2, as the thickness decreases to about half, the grain boundary resistance decreases more than half, the grain boundary capacitance has little increase, which is due to the sample not being uniform. The scanning electron microscope (SEM) image of the sample is shown in Figure 48.

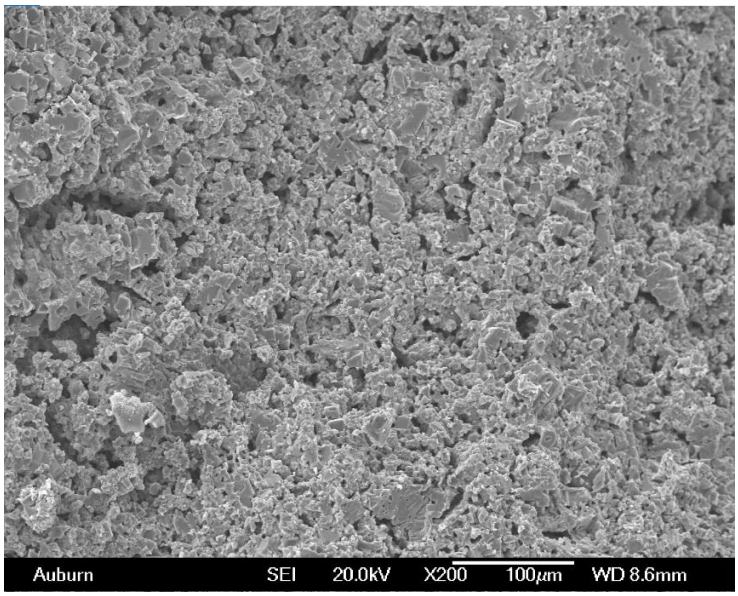

Figure 48. SEM image of $Li_{1.3}Al_{0.3}Ti_{1.7}(PO_4)_3$ sample.

From the SEM image, there are many pores with different sizes and cracks in the sample which show the nonuniformity, some parts of the sample may have more grain boundaries or fewer grain boundaries. The nonuniformity may cause grain boundary resistance (R2) is not exactly proportional to the thickness, and the grain boundary capacitance CPE2 are not exactly the same after grinding from 0.45 cm to 0.23 cm.

The capacitor (CPE1) is geometry capacitor caused by two parallel silver electrodes. As the thickness decreases, in other words, the distance between the two electrodes decreases, the geometry capacitance increases as expected. According to the capacitance equation for a parallel plate capacitor:

$$C = \frac{\varepsilon A}{d} \qquad (4.6.1.2)$$

where C is capacitance, ε is permittivity, A is area, d is the distance between two parallel plates, and C is proportional to 1/d. From the data in Table 3, as the thickness decreases from 0.45 cm to 0.23 cm, the CPE1 increases from $8.6x10^{-11}$ to $2.2x10^{-10}$ with deviation 113% and 100% respectively which follows the relation $C \propto 1/d$ by considering the deviations. However, the values of CPE1 are too small and the deviation is large compared with other elements, so they cannot represent the actual values of CPE1.

4.6.2 Change in Sintering Time

In order to know how sintering time will change the microstructure of LATP samples, and if the change can be revealed by the equivalent circuit model as predicted, the LATP samples were prepared with a different sintering time of 900℃ for 6 hours and 14 hours respectively. The SEM images of each are shown in Figure 49-50.

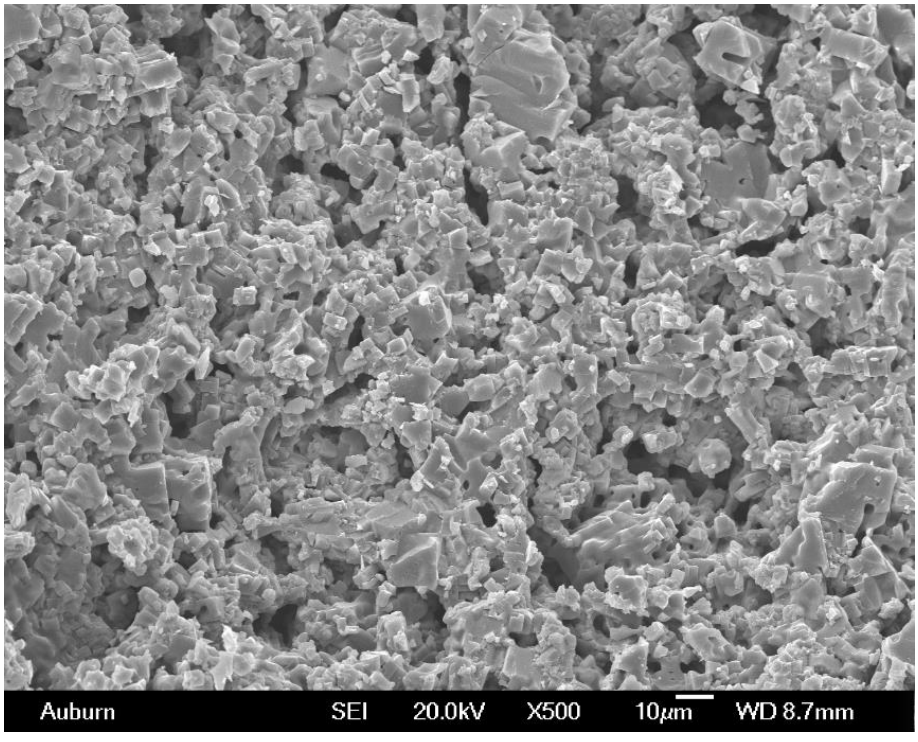

Figure 49. SEM image of LATP with 900℃-6h sintering.

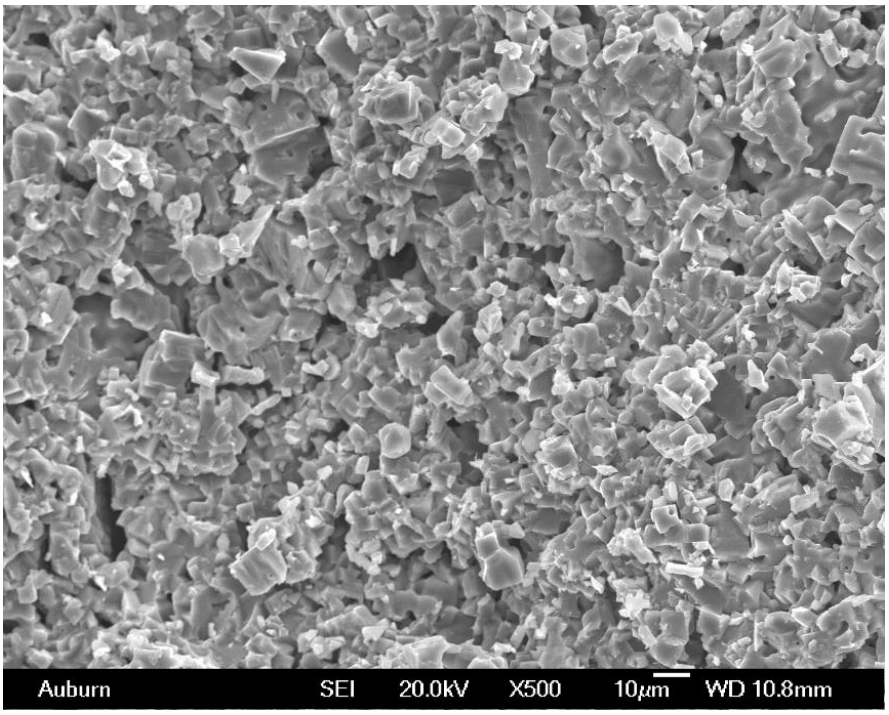

Figure 50. SEM image of LATP with 900℃-14h sintering.

Compare these two images, the sample with 6h sintering time has more pores or free space among particles. There are fewer contacts among these particles which means there are fewer grain boundaries. So, there are fewer channels for ions to transfer through the sample. The sample with 14h sintering time has fewer pores, more particles are sintered together, and the density increased. There are more contacts among particles which means there are more grain boundaries. Even though grain boundaries are barriers for ions to transfer in ceramic and more resistive than grains, the sample with 16h sintering time should have lower grain boundary resistance because more pores are replaced by grain boundaries that provide more channels for ions to transfer. In addition, the compact structure allows particles to have larger contact areas with each other. For ions to transfer through grain boundary from grain to grain, a larger contact area means a larger grain boundary area. According to the equation 3.5.1.1, $R \propto 1/A$, larger grain boundary area has a lower grain boundary resistance.

The impedance spectrums of samples with 6h and 14h sintering time are compared in the same complex plan and shown in Figure 51-54.

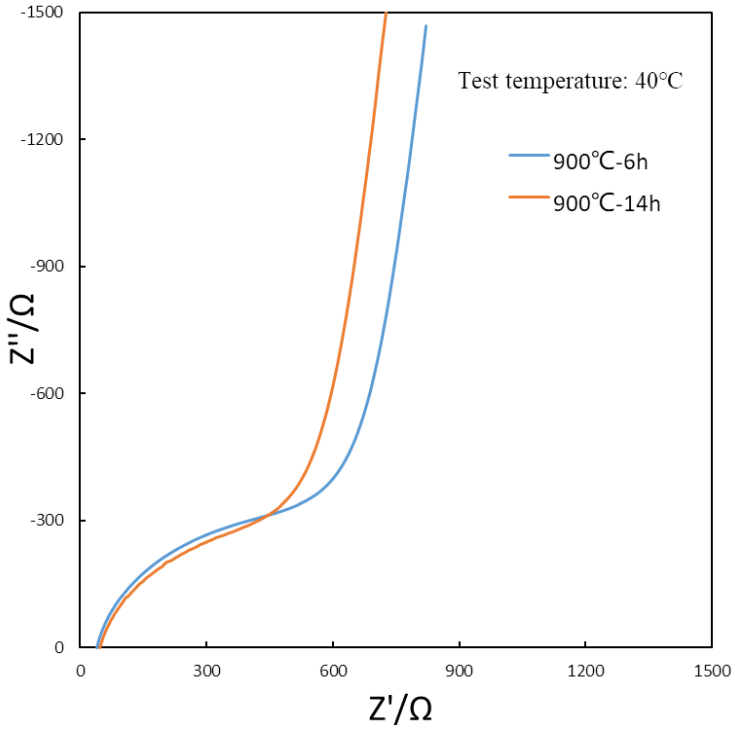

Figure 51. Nyquist plots of LATP samples with different sintering time at 40℃.

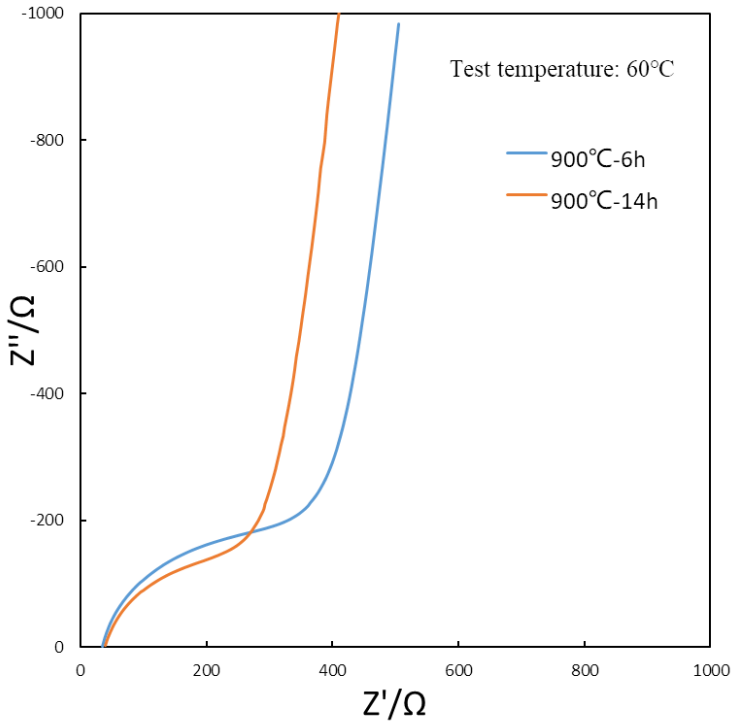

Figure 52. Nyquist plots of LATP samples with different sintering time at 60℃.

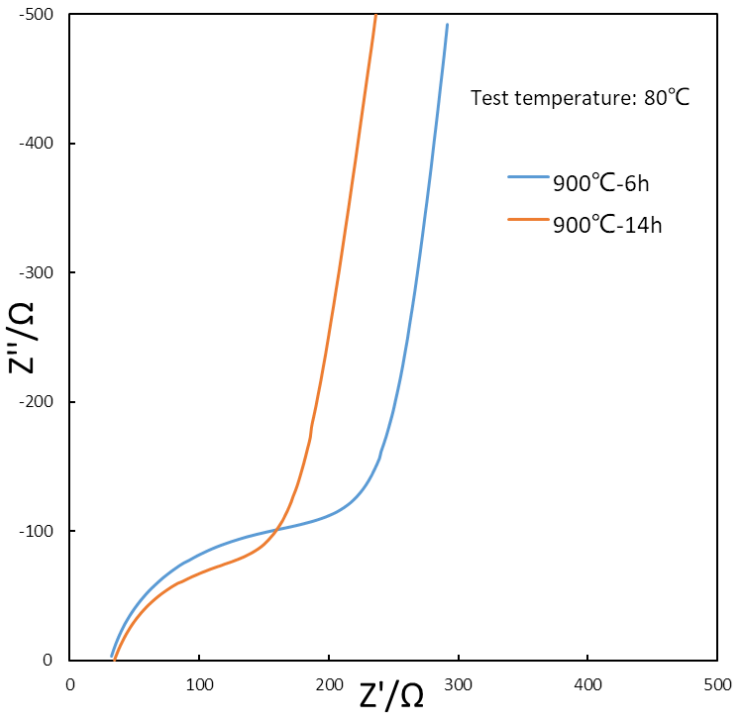

Figure 53. Nyquist plots of LATP samples with different sintering time at 80℃.

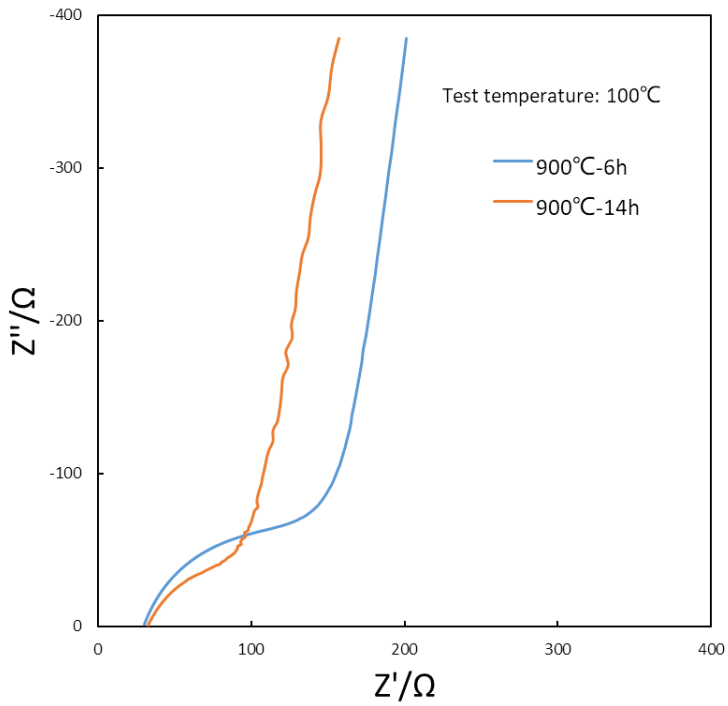

Figure 54. Nyquist plots of LATP samples with different sintering time at 100℃.

From the figures above, the impedance plots of the sample with 900℃-14h sintering condition have a little larger intercept with the Z' axis which means they have a larger bulk resistance than the sample with 900℃-6h sintering condition. Grain boundary resistance usually can be estimated by the intercept of the semicircle on the Z' axis. The sample with 900℃-14h sintering condition has a smaller semicircle and intercept, which means the sample has smaller grain boundary resistance than the sample with 900℃-6h.

The impedance plots were fitted by the equivalent circuit, and the fitted curves show high coincidence as figures in chapter 4.4. Both bulk and grain boundary resistance were read from the fitted results, and the conductivities of both were calculated by the equation (4.3.3). Table 4-5 show the values of resistance and conductivity at different temperatures.

Table 4. Resistance and conductivity of NASICON sample with 900℃-6h sintering.

t/℃	R_b/Ω	R_{gb}/Ω	σ_b/Scm-1	σ_{gb}/Scm-1
40	23.4	662.5	0.0041	0.00014
60	15.2	401.5	0.0063	0.00024
80	9.0	244.9	0.0106	0.00039
100	7.3	154.2	0.0131	0.00062

Table 5. Resistance and conductivity of NASICON sample with 900℃-14h sintering.

t/℃	R_b/Ω	R_{gb}/Ω	σ_b/Scm-1	σ_{gb}/Scm-1
40	29.5	574.3	0.0043	0.00022
60	23.4	299.8	0.0054	0.00042
80	17.7	171.9	0.0071	0.00073
100	7.9	93.1	0.0159	0.00135

From Table 4 and Table 5, samples with a 6h and 14h sintering time do not have an obvious change in bulk conductivity. However, it has higher grain boundary conductivity than the sample with a 6h sintering time which is expected from the SEM images of the two samples. And thus, the increased grain boundary conductivity caused by increased sintering time is revealed by the equivalent circuit.

Chapter 5

Conclusions

The electrical impedance spectroscopy results for the β-alumina and LATP electrolytes can be modeled with an equivalent circuit to separate the contributions from the bulk resistance and the grain boundary resistance.

A general equivalent circuit was created to conduct the fitting process which eliminates the external factors which usually exist in the EIS testing process including the system resistance, the inductance caused by wire bending, the geometrical capacitance due to the electrolyte between the two parallel metal electrodes, and the interface capacitance caused by two electrolyte-electrode interfaces. This equivalent circuit can be simplified according to the conditions of the experiment.

The thickness and the sintering time of samples were changed to show the changes in the contribution of different components as predicted by the equivalent circuit. As the thickness decreases, the electrode-electrolyte interface capacitance does not change and the geometry capacitance CPE1 decreases as expected. Similarly, as the sintering time increases, the bulk conductivity does not change, and the grain boundary conductivity increases as expected. These results support the proposed physical significance of each equivalent circuit component.

References

[1] Lasia, Andrzej. Electrochemical impedance spectroscopy and its applications. Vol. 7. New York: Springer, 2014.

[2] Ray, Brian M. "A study of the lithium ionic conductor Li5La3Ta2O12: from synthesis through materials and transport characterization." (2014).

[3] Gönüllü, Yakup, et al. "Equivalent circuit models for determination of the relation between the sensing behavior and properties of undoped/cr doped TiO2 NTs." Chemosensors 2.1 (2014): 69-84.

[4] Huang, Jun. "Diffusion impedance of electroactive materials, electrolytic solutions and porous electrodes: Warburg impedance and beyond." Electrochimica Acta 281 (2018): 170e188.

[5] Powers, R. W., and S. P. Mitoff. "An Analysis of the Impedance of Polycrystalline Beta-Alumina." Journal of The Electrochemical Society 122.2 (1975): 226-231.

[6] Hooper, A. "A study of the electrical properties of single-crystal and polycrystalline β-alumina using complex plane analysis." Journal of Physics D: Applied Physics 10.11 (1977): 1487.

[7] De Jonghe, Lutgard C. "Grain boundaries and ionic conduction in sodium beta alumina." Journal of Materials Science 14.1 (1979): 33-48.

[8] Duluard, Sandrine, et al. "Lithium conducting solid electrolyte Li1. 3Al0. 3Ti1. 7 (PO4) 3 obtained via solution chemistry." Journal of the European Ceramic Society 33.6 (2013): 1145-1153.

[9] Zhao, Erqing, et al. "Pechini synthesis of high ionic conductivity Li1. 3Al0. 3Ti1. 7 (PO4) 3 solid electrolytes: The effect of dispersant." Journal of Alloys and Compounds 680 (2016): 646-653.

[10] Arbi, K., J. M. Rojo, and J. Sanz. "Lithium mobility in titanium based Nasicon Li1+ xTi2− xAlx (PO4) 3 and LiTi2− x Zrx (PO4) 3 materials followed by NMR and impedance spectroscopy." Journal of the European Ceramic Society27.13-15 (2007): 4215-4218.

[11] Kumar, Binod, and Joykumar S. Thokchom. "Space charge signature and its effects on ionic transport in heterogeneous solids." Journal of the American Ceramic Society 90.10 (2007): 3323-3325.

[12] Xu, Xiaoxiong, et al. "High lithium ion conductivity glass-ceramics in Li2O–Al2O3–TiO2–P2O5 from nanoscaled glassy powders by mechanical milling." Solid State Ionics 177.26-32 (2006): 2611-2615.

[13] Fu, Jie. "Superionic conductivity of glass-ceramics in the system Li 2O-Al 2O 3-TiO 2-P 2O 5." Solid State Ionics 96.3-4 (1997): 195-200.

[14] Kosova, N. V., et al. "Lithium conductivity and lithium diffusion in NASICON-type Li 1+ x Ti 2–x Al x (PO 4) 3 (x= 0; 0.3) prepared by mechanical activation." Ionics 14.4 (2008): 303-311.

[15] Huggins, R. A. "Simple Method to Determine Electronic Conductivity in Mixed and Ionic Components of the Conductors." Ionics 8 (2002): 300-313.

[16] Song, Guangling. "Equivalent circuit model for AC electrochemical impedance spectroscopy of concrete." Cement and concrete research 30.11 (2000): 1723-1730.

[17] Jensen, Finn. "Activation energies and the Arrhenius equation." Quality and Reliability Engineering International 1.1 (1985): 13-17.

[18] Will, F. G. "Effect of water on beta alumina conductivity." Journal of The Electrochemical Society 123.6 (1976): 834-836.

[19] Irvine, John TS, Derek C. Sinclair, and Anthony R. West. "Electroceramics: characterization by impedance spectroscopy." Advanced Materials 2.3 (1990): 132-138.

[20] Bohnke, O., S. Ronchetti, and D. Mazza. "Conductivity measurements on nasicon and nasicon-modified materials." Solid State Ionics 122.1-4 (1999): 127-136.

[21] Aono, Hiromichi, et al. "Ionic conductivity of solid electrolytes based on lithium titanium phosphate." Journal of the electrochemical society 137.4 (1990): 1023-1027.

[22] Ren, Yaoyu, et al. "Oxide electrolytes for lithium batteries." Journal of the American Ceramic Society 98.12 (2015): 3603-3623.

Appendix

1. **Bode fitting results of β-alumina are shown in Figure 55-62.**

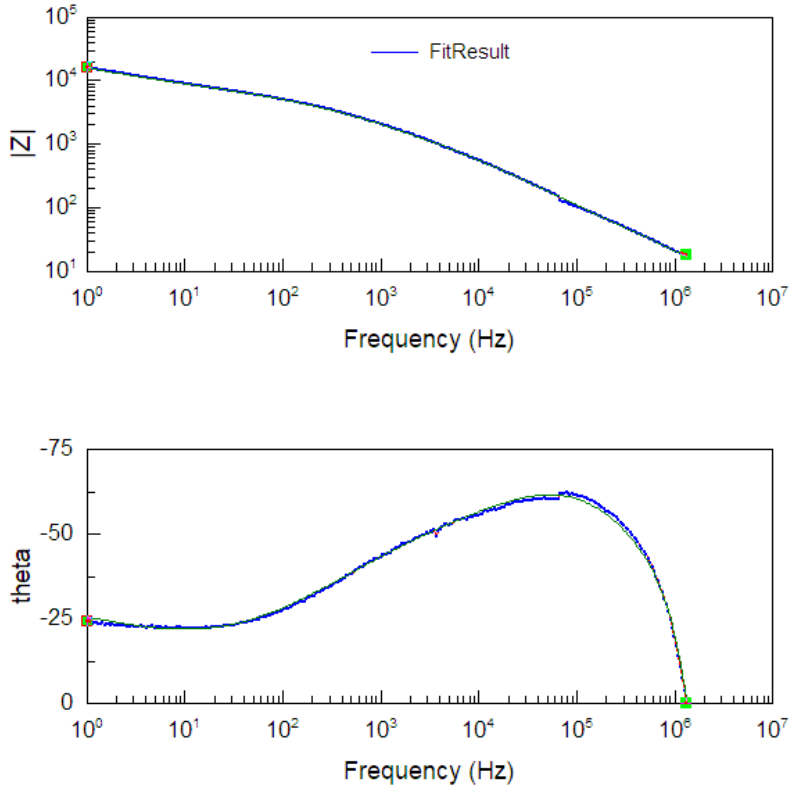

Figure 55. Bode plots and fitting results of β-alumina at 20°C.

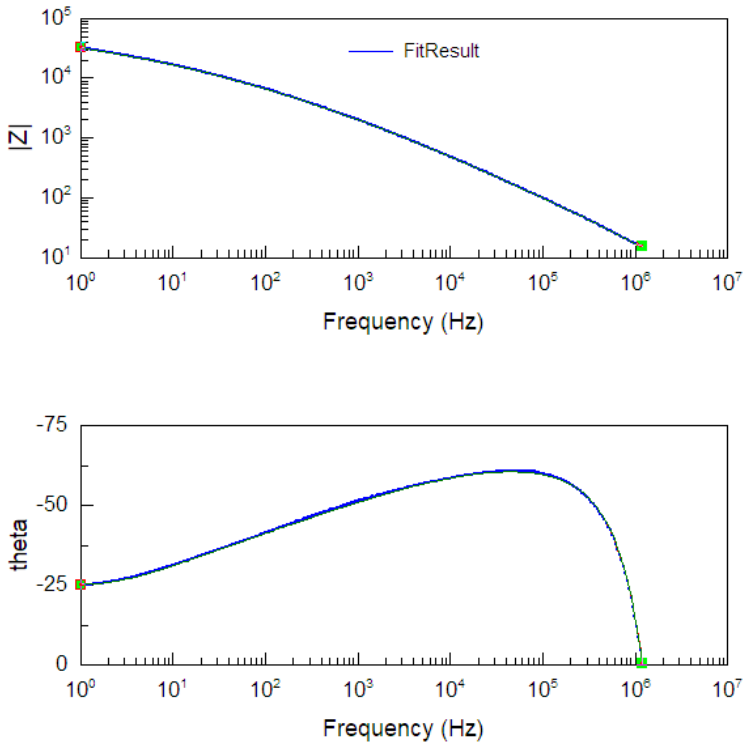

Figure 56. Bode plots and fitting results of β-alumina at 50°C.

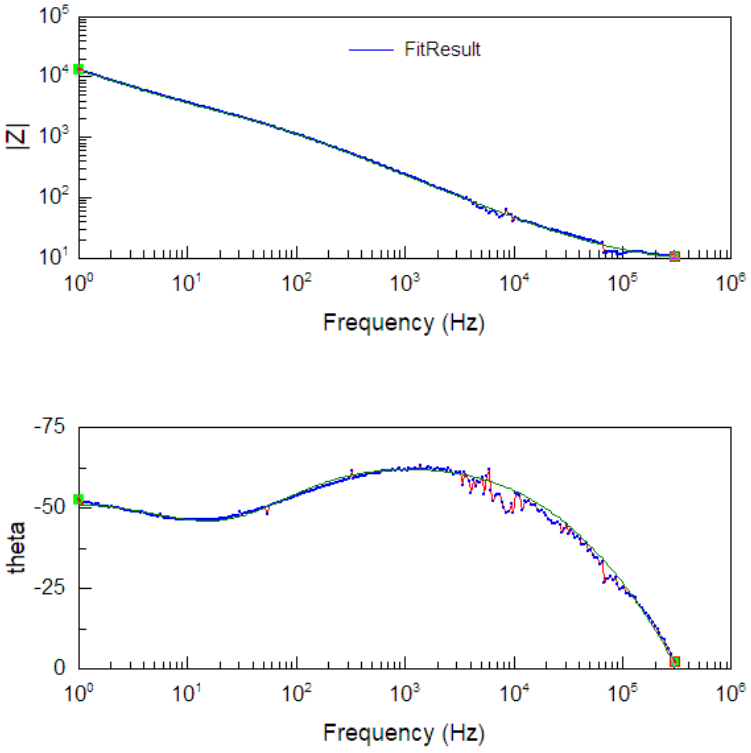

Figure 57. Bode plots and fitting results of β-alumina at 100°C.

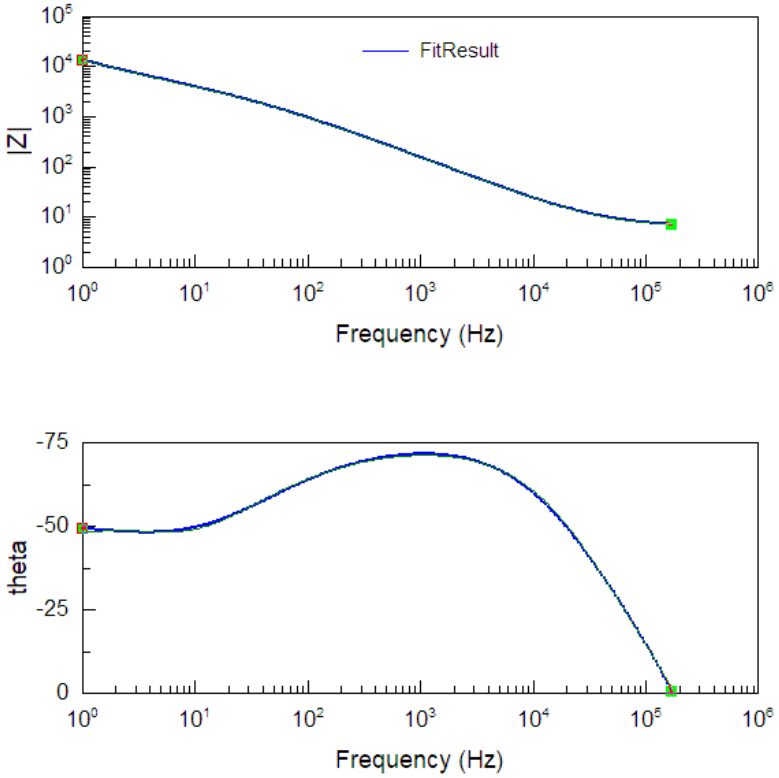

Figure 58. Bode plots and fitting results of β-alumina at 150°C.

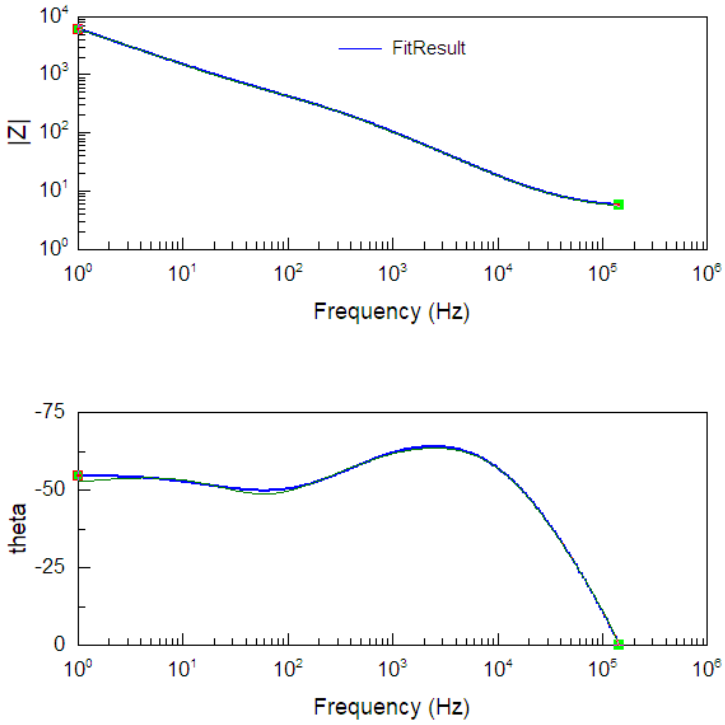

Figure 59. Bode plots and fitting results of β-alumina at 200°C.

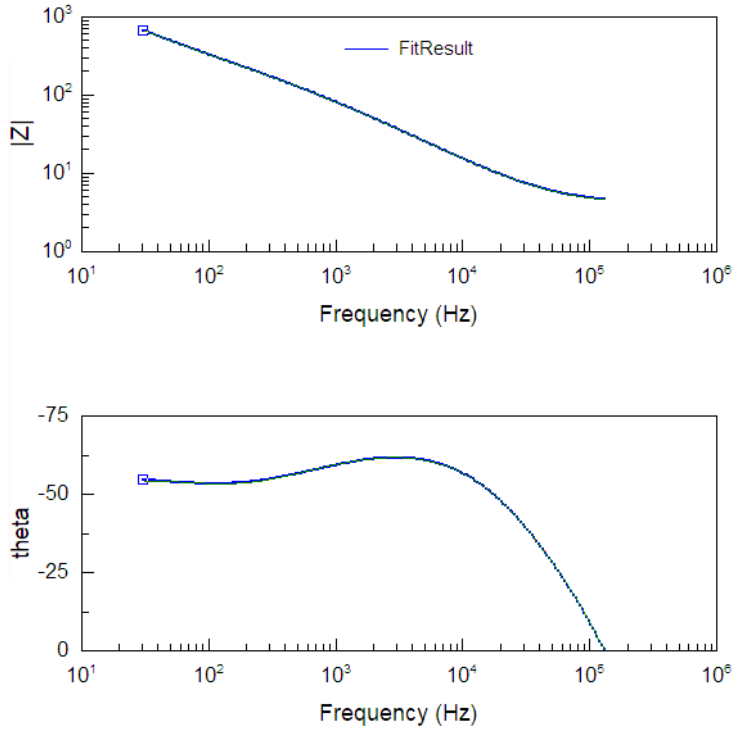

Figure 60. Bode plots and fitting results of β-alumina at 250°C.

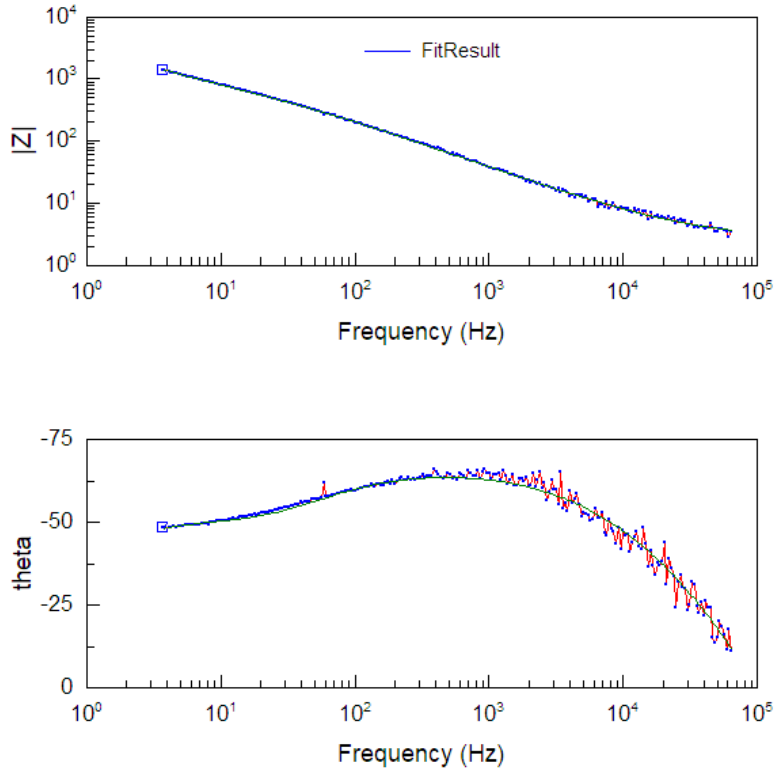

Figure 61. Bode plots and fitting results of β-alumina at 300°C.

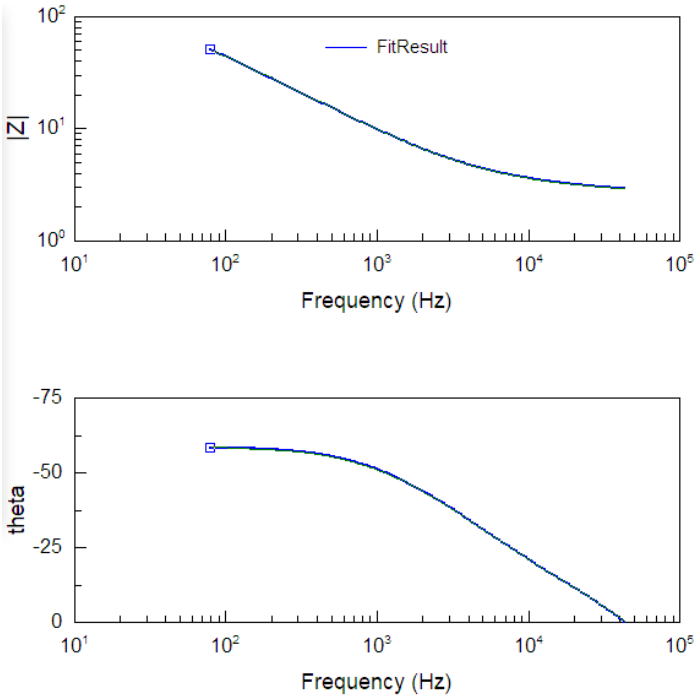

Figure 62. Bode plots and fitting results of β-alumina at 350℃.

2. Bode fitting results of LATP are shown in Figure 63-67.

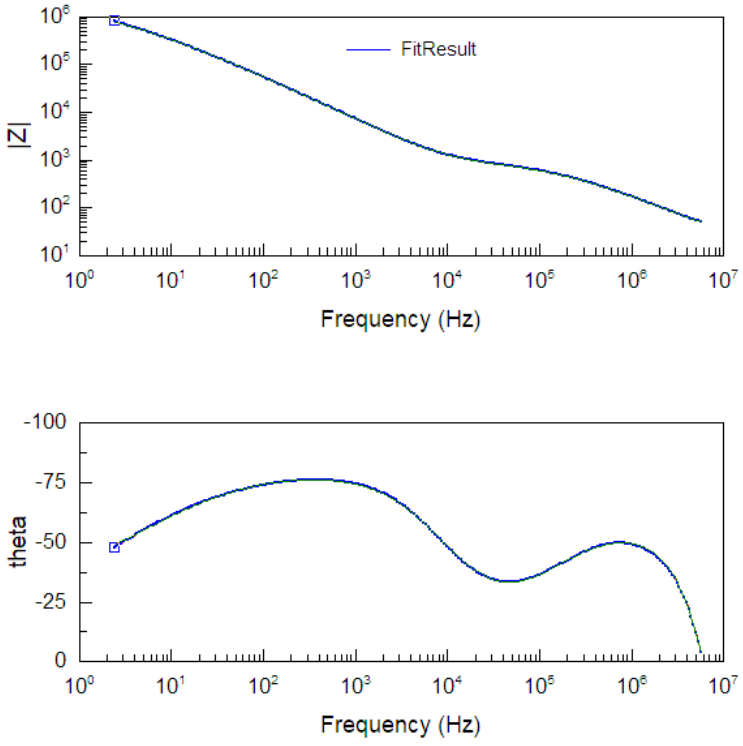

Figure 63. Bode plots and fitting results of LATP at 20℃.

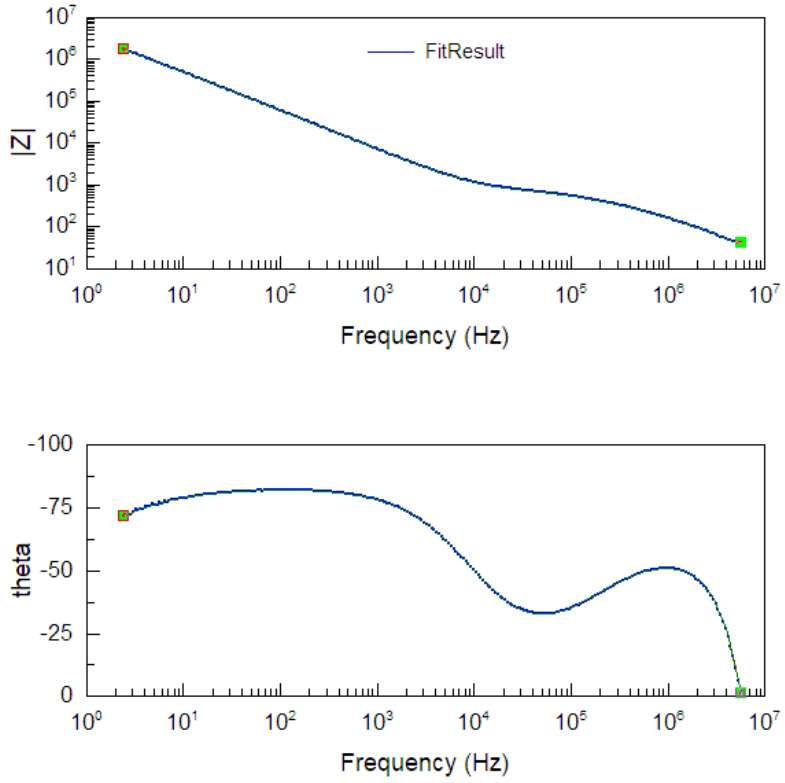

Figure 64. Bode plots and fitting results of LATP at 40°C.

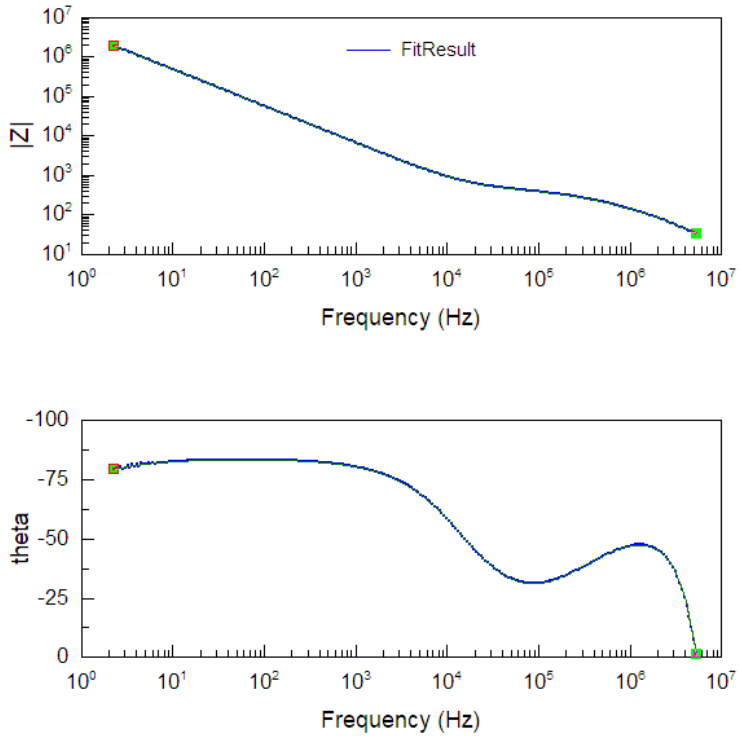

Figure 65. Bode plots and fitting results of LATP at 60°C.

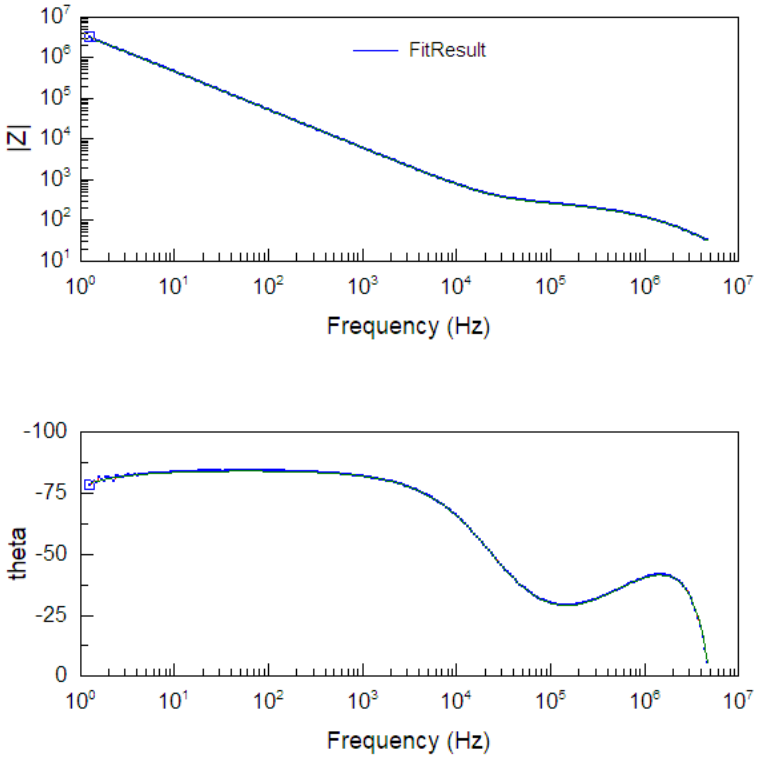

Figure 66. Bode plots and fitting results of LATP at 80°C.

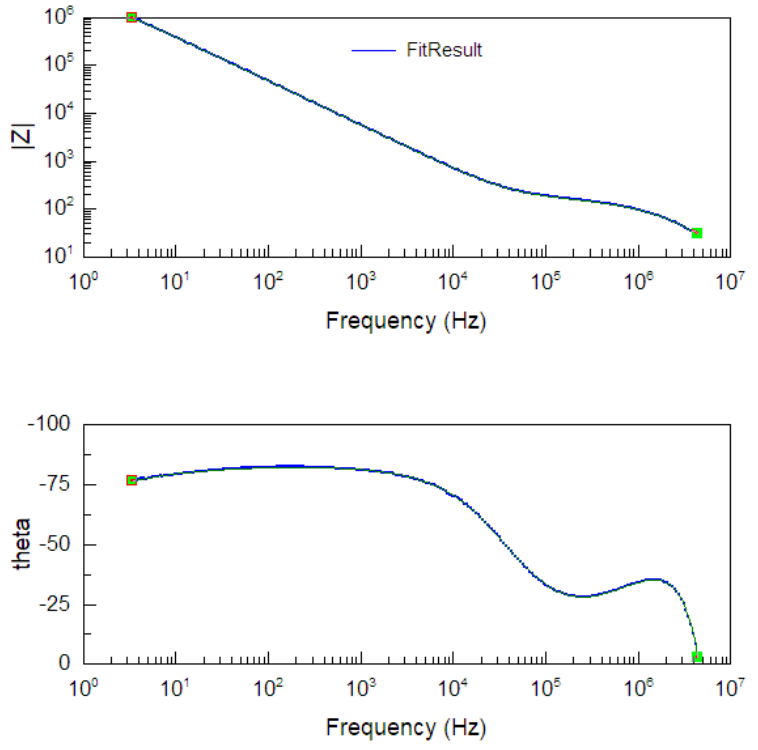

Figure 67. Bode plots and fitting results of LATP at 100°C.